Geochemistry Geophysics Geosystems G3

Article
Volume 00, Number 00
0 MONTH 2013
doi: 10.1002/ggge.20160
ISSN: 1525-2027

Published by AGU and the Geochemical Society

The spatial and temporal evolution of strain during the separation of Australia and Antarctica

Philip Ball
Fault Dynamics Research Group, Department of Earth Sciences, Royal Holloway, University of London, Egham, UK

Now at ConocoPhillips, 600 North Dairy Ashford, OF3064, Houston, Texas, 77079, USA (Philip.j.ball@conocophillips.com)

Graeme Eagles
Fault Dynamics Research Group, Department of Earth Sciences, Royal Holloway, University of London, Egham, UK

Now at Alfred Wegener Institute for Polar and Marine Research, Bremerhaven, Germany

Cynthia Ebinger
Fault Dynamics Research Group, Department of Earth Sciences, Royal Holloway, University of London, Egham, UK

Now at Department of Earth and Environmental Sciences, University of Rochester, Rochester, New York, USA

Ken McClay
Fault Dynamics Research Group, Department of Earth Sciences, Royal Holloway, University of London, Egham, UK

Jennifer Totterdell
Petroleum and Marine Division, Geoscience Australia, Canberra, Australia

[1] A re-evaluation of existing onshore and offshore gravity, magnetic, seismic reflection, and well data from the Australo-Antarctic margins suggests that magmatism and along-strike lithospheric heterogeneities have influenced the localization of initial rifting. The 3-D crustal architecture of the Australian and Antarctic margins, which formed during multiple rifting episodes spanning ~80 Myr, reveal local asymmetries along strike. Rift structures from the broad, late Jurassic (165–145 Ma) rift zone are partially overprinted by a narrower, mid-to-late Cretaceous rift zone (~100 Ma), which evolved in highly extended crust. This late-stage rift zone is located within a region of heterogeneous crust with faults that cut late syn-rift strata, interpreted as a continent ocean transition zone. This late stage transitional rift is populated by seismically identified rift-parallel basement highs and intracrustal bodies with corresponding positive Bouguer gravity and magnetic anomalies. These undrilled features can be interpreted as exposures of exhumed mantle rocks, lower crustal rocks and/or as discrete magmatic bodies. Our results suggest that strain across an initially broad Australo-Antarctic rift system (165–145 Ma) migrated to a narrow rift zone with some magmatism at 100–83 Ma. Breakup did not occur until ~53 Ma within the eastern Bight-Wilkes and Otway-Adélie margin sectors, suggesting a west to east propagation of seafloor spreading. The prolonged eastward propagation of seafloor spreading processes and the increased asymmetry of the Australian-Antarctic margins coincides with a change from rift-perpendicular to oblique rifting processes, which in turn coincide with along-strike variations in cratonic to Palaeozoic lithosphere.

Components: 18,027 words, 11 figures, 3 tables.

Keywords: Australia; Antarctica; rift; evolution; tectonics; margins.

Index Terms: 8105 Continental margins: divergent: Tectonophysics; 8109 Continental tectonics: extensional: Tectonophysics; 8106 Continental margins: transform: Tectonophysics; 8149 Planetary tectonics: Tectonophysics; 8178 Tectonics and magmatism: Tectonophysics.

Received 2 January 2013; **Revised** 15 April 2013; **Accepted** 27 April 2013; **Published** 00 Month 2013.

Ball, P., G. Eagles, C. Ebinger, K. McClay, and T. Totterdell, (2013), The spatial and temporal evolution of strain during the separation of Australia and Antarctica, *Geochem. Geophys. Geosyst., 14,* doi:10.1002/ggge.20160.

1. Introduction

[2] Analytic and numerical models show that continental thinning leading to breakup may be initiated through mechanical thinning and weakening of the lithosphere, depth-dependent extension, and magmatism as rifting progresses toward rupture [e.g., *McKenzie*, 1978; *Whitmarsh et al*., 2001; *Davis and Kusznir*, 2004; *Buck*, 2004; *Yamasaki and Gernigon*, 2009; *Huismans and Beaumont*, 2011]. At the regional scale it is evident that crustal and lithospheric rheological heterogeneities such as preexisting weak and strong zones may influence these processes by localizing in-plane stresses [e.g., *Dunbar and Sawyer*, 1989; *Bassi*, 1995; *Vauchez et al*., 1997; *Petit and Ebinger*, 2000; *Corti et al*., 2003; *Muntener and Manatschal*, 2006]. The relative roles, and the evolutionary interplay, of these influences on rift zone segmentation are debated, in large part owing to the lack of models and constraints on the along-strike variations in structure [e.g., *Hayward and Ebinger*, 1996; *Behn and Lin*, 2000; *Buck*, 2004; *van Wijk and Blackman*, 2005; *Lizarralde et al*., 2007].

[3] Insights into the late-stage evolution of rifts and rifted margins have emerged from detailed deep sea drilling, seismic reflection, refraction, and field studies of the weakly magmatic Iberia-Newfoundland and Alpine margins and of the East African Rift system [e.g., *Reston et al*., 1996; *Whitmarsh et al*., 2001; *Pérez-Gussinyé et al*., 2001; *Manatschal*, 2004; *Péron-Pinvidic and Manatschal*, 2009; *Lavier and Manatschal*, 2006; *Reston*, 2007; *van Avendonk et al*., 2009; *Keir et al*., 2009; *Keranen et al*., 2009; *Bronner et al*., 2011]. These studies provided detailed 2-D concepts for the distribution of strain as rifting progresses to seafloor spreading, but along-strike variability has been interpreted primarily in terms of transform segmentation of transtensional margins [e.g., *d'Acremont et al*., 2005; *Lizarralde et al*., 2007; *Leroy et al*., 2010]. The presence or absence of melt along the strike of the rift is a strong determinant of the rift architecture, and incipient transform faults may guide or restrict the movement of magma [e.g., *Shillington et al*., 2009; *Leroy et al*., 2010]. While there are many different factors influencing rift evolution, 3-D numerical models show that a change from rift-perpendicular to oblique extension facilitates the rifting process because it requires less force to reach the plastic yield limit [*Brune et al*., 2012]. Such changes may occur after a period of quiescence as fault systems reorganize [e.g., *Ebinger et al*., 2013].

[4] Combined onshore-offshore geophysical data from the ~4000 km long southern Australian and conjugate Antarctic margins provide an opportunity to characterize the evolution and distribution of strain and magmatism as extension progressed to seafloor spreading. Long-offset seismic reflection profiles across the Australian and Antarctic margins (Figure 1) have been interpreted by several teams, resulting in a number of asymmetric or symmetric breakup models featuring exhumed mantle wedges, serpentinite bodies, and/or magmatic material [e.g., *Wannesson et al*., 1985; *Eittreim et al*., 1985; *Eittreim and Smith*, 1987; *Eittreim*, 1994; *Wannesson*, 1991; *Sayers et al*., 2001; *De Santis et al*., 2003; *Colwell et al*., 2006; *Direen et al*., 2007; *Stagg and Reading*, 2007; *Direen et al*., 2011, 2012; *Espurt et al*., 2012]. Several recent interpretations have been supplemented by along-profile potential field interpretations [e.g., *Sayers et al*., 2001; *Colwell et al*., 2006; *Direen et al*., 2007, 2011, 2012]. Many of these interpretations have been completed under the assumption that the margins are magma poor, because seaward dipping reflectors that typify volcanic margins are not present and because

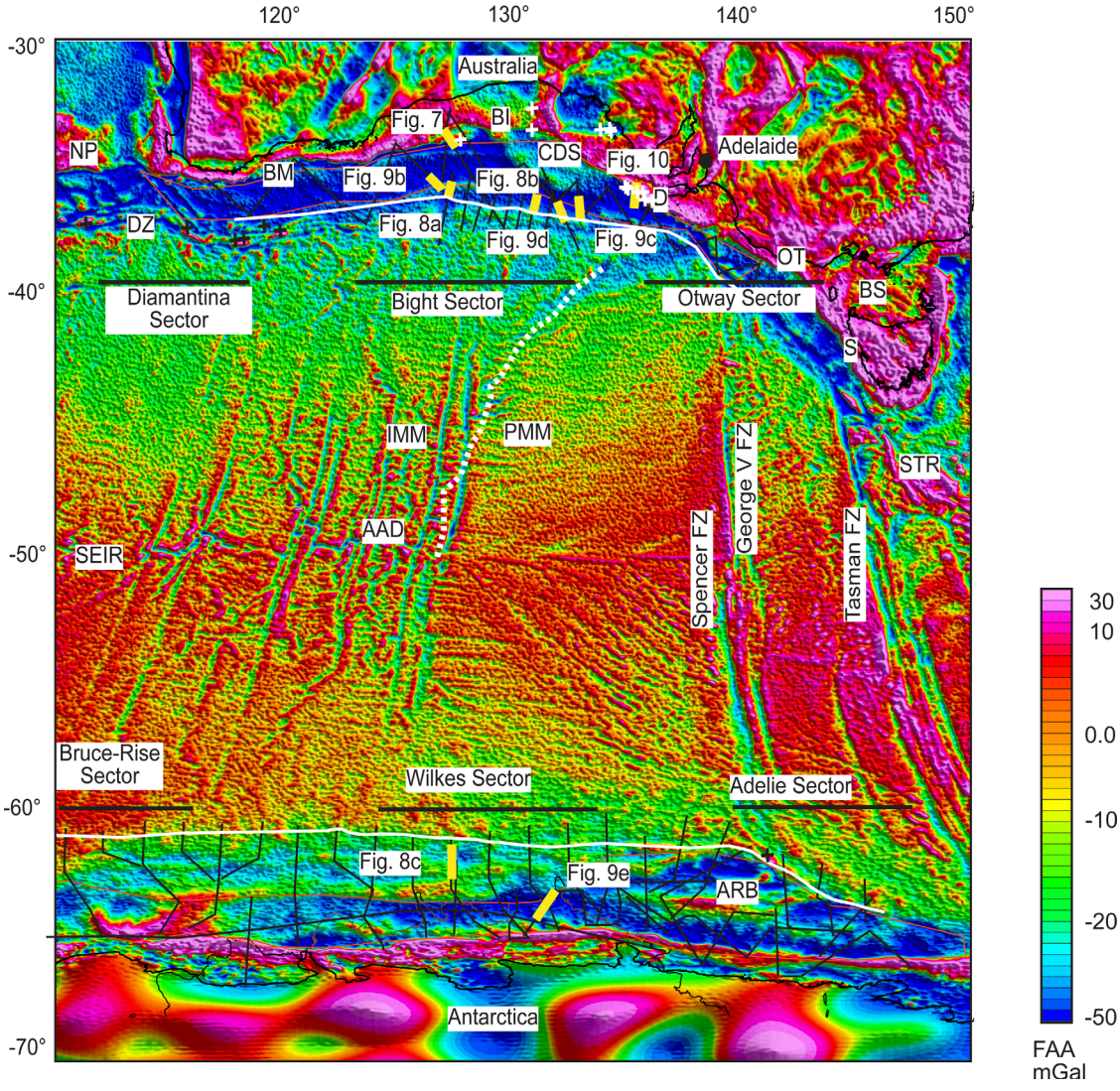

Figure 1. Satellite derived free-air gravity anomalies of the Australian-Antarctic passive margins [*Sandwell and Smith*, 1997, 2009]. The conjugate margin is subdivided into the Diamantina-Bruce Rise Sector, the Bight-Wilkes Margin Sector and the Otway-Sorell-Adélie Sector which are characterized by distinct structural and stratigraphic patterns. Exploration wells used in this study are marked by white crosses. Long offset seismic reflection lines shown by black lines for the Australia and Antarctic margins. Yellow markers indicate the sector and location of the seismic line that is used in the respective figures. Black crosses: dredge samples, see text, and *Borissova* [2002] for more details. White solid line: Continent Ocean Boundary: COB; White dashed line: boundary between Indian and Pacific-type mantle [after *Christie et al*., 2004]. IMM: Indian (ocean) MORB Mantle (isotopically defined); PMM: Pacific (ocean) MORB mantle (isotopically defined) after *Christie et al*. [2004]. AAD: Australian-Antarctic discordance; ARB: Adélie rift block; BS: Bass Strait; BI: Bight basin; BM: Bremer basin; D: Duntroon basin; DZ: Diamantina zone; CDS: Ceduna delta system; FZ: Fracture zone; NP: Naturaliste plateau; OT: Otway basin; S: Sorell basin; SEIR: South East Indian ridge; STR: South Tasman Rise; Projection: Mercator Projection, Ellipsoid: WGS84.

continental peridotites that feature at magma-poor margins have been dredged at the western and eastern extremes of the Australian and Antarctic margins [*Nicholls et al*., 1981; *Yuasa et al*., 1997; *Beslier et al*., 2004, Figure 1]. Stepping back from these largely 2-D models, and the assumption of amagmatic rifting, we reinterpret the seismic reflection and potential field data all along the margins. The resulting 3-D perspective enables us to compare and contrast the margin structure that develops in cratonic and Phanerozoic lithosphere, and with and without syn-rift magmatism.

[5] This 3-D perspective, presented within a regional plate reconstruction context, suggests that

breakup was diachronous along strike, was influenced by pre-existing lithospheric heterogeneities, and involved a basinward jump in the locus of strain and probably magmatism ~10–20 Myr prior to the onset of sustained seafloor spreading. The resulting narrow, late stage rift zone adopted a new segmentation pattern that was influenced by prerift structures, and locally, by magmatic processes.

1.1. Tectonic Setting

[6] A first period of extension affected the margins at 165–145 Ma, forming en-echelon half-graben systems of the Bight and Otway basins south of Australia [*Totterdell et al*., 2000; *Krassay et al*., 2004; *Bradshaw et al*., 2005; *Blevin*, 2005; *Blevin and Cathro*, 2008; *Totterdell and Bradshaw*, 2004]. The western parts of this rift formed in Mesoproterozoic and Neoproterozoic mobile belts where the lithosphere is 180–250 km thick and crustal thicknesses vary between 30 and 45 km [*O'Reilly and Griffin*, 2006; *Gaul et al*., 2003; *Clitheroe et al*., 2000; *von Frese et al*., 1999]. The Gawler-Mawson craton in the central portion of the reconstructed margins is a complex melange of Mesoproterozoic and Archaean rocks [*Fitzsimons*, 2003] (Figure 2). East of the deeply rooted craton, the Australian-Antarctic lithosphere is dominated by Phanerozoic (Ross-Delamerian, Lachlan and New England) mobile belts where the lithosphere is 80–150 km thick and crustal thicknesses vary between 30 and 50 km [*Cleary*, 1973; *Danesi and Morelli*, 2000; *Drummond and Collins*, 1986; *Fishwick et al*., 2005; *Ritzwoller et al*., 2001; *Clitheroe et al*., 2000; *Simons et al*., 1999; *von Frese et al*., 1999; *Simons and van der Hilst*, 2002]. These eastern reaches were heated and intruded at 190–170 Ma [e.g., *Hergt et al*., 1991; *Elburg and Soesoo*, 1999; *Foden et al*., 2002, Figure 2]. The present-day eastward decrease in plate strength shown by gravity-isostasy studies [*Zuber et al*., 1989; *Simons and van der Hilst*, 2002] is likely to date from at least 190 Ma, and likely before.

[7] Trace element analysis and isotopic analyses indicate the approximate location of the long-lived pre-100 Ma western Pacific subduction zone beneath the margins (Figure 1). This geochemical line marks the approximate boundary between domains of Indian and Pacific mantle, and is thought to be largely responsible for the present-day Australian-Antarctic discordance (AAD) on the South East Indian ridge (SEIR) (Figure 1) [*Christie et al*., 2004; *Whittaker et al*., 2010]. Geodynamic models suggest that the late stages of rifting, breakup and early seafloor spreading may have been influenced by the subducted Mesozoic slab and its volatile-rich mantle wedge [*Gurnis et al*., 1998; *Gurnis and Müller*, 2003; *Whittaker et al*., 2010].

[8] In part owing to the deepwater setting of the Bight Basin, the rift, breakup and early seafloor spreading stages are the subject of much discussion because the sources, and the ages, of the magnetic reversal anomalies that frame the outer edges of the margin are not fully agreed upon [e.g., *Cande and Mutter*, 1982; *Tikku and Cande*, 1999; *Sayers et al*., 2001; *Whittaker et al*., 2007]. By ~45 Ma, Australian–Antarctic plate divergence was fast enough to produce indisputable magnetic reversal anomalies in oceanic crust. These anomalies are flanked by areas of subdued magnetic response in which the presence of further reversal anomalies as old as 84 Ma is debated.

[9] Landward, the magnetic quiet zone (MQZ) is the site of continued uncertainty regarding rift related structures and the nature of the crust (Figure 1). Early geophysical studies established the presence of highly attenuated continental crust to which there has been little or no magmatic addition during rifting [e.g., *Weissel and Hayes*, 1972; *Talwani et al*., 1978; *Konig*, 1987; *Childs and Stagg*, 1987; *Eittreim* 1994]. Several interpreters propose that the oceanward limit of the MQZ marks the onset of oceanic crust, within which the earliest poorly correlatable magnetic anomalies are indicative of extremely slow spreading rates [*Tikku and Cande*, 1999; *Tikku and Direen*, 2008; *Whittaker et al*., 2007]. By analogy to the drilled Iberia-Newfoundland margins [e.g., *Whitmarsh et al*, 2001; *Sibuet et al*., 2007], basement highs within and along the edge of the MQZ would be ridges of exhumed mantle rocks and/or magmatic intrusions within the highly attenuated continental crust, although precise interpretations differ [e.g., *Sayers et al*., 2001; *Ball* 2005; *Colwell et al*., 2006; *Direen et al*., 2007, 2011]. Distinguishing between these interpretations has important implications for the timing of breakup, for the distribution and timing of strain prior to and during plate rupture, and for the heatflow and subsidence history of the margin.

[10] Previous studies of continental rupture focussed on the evolving geometry of 2-D regional seismic and gravity profiles of the conjugate Australia and/or Antarctic margins. *Eittreim et al*. [1985] and *Moore and Eittreim* [1987] suggested that break up left asymmetrical margins through a "crustal sliding" model involving the evolution of multiple crustal detachments. *Lister et al*. [1986]

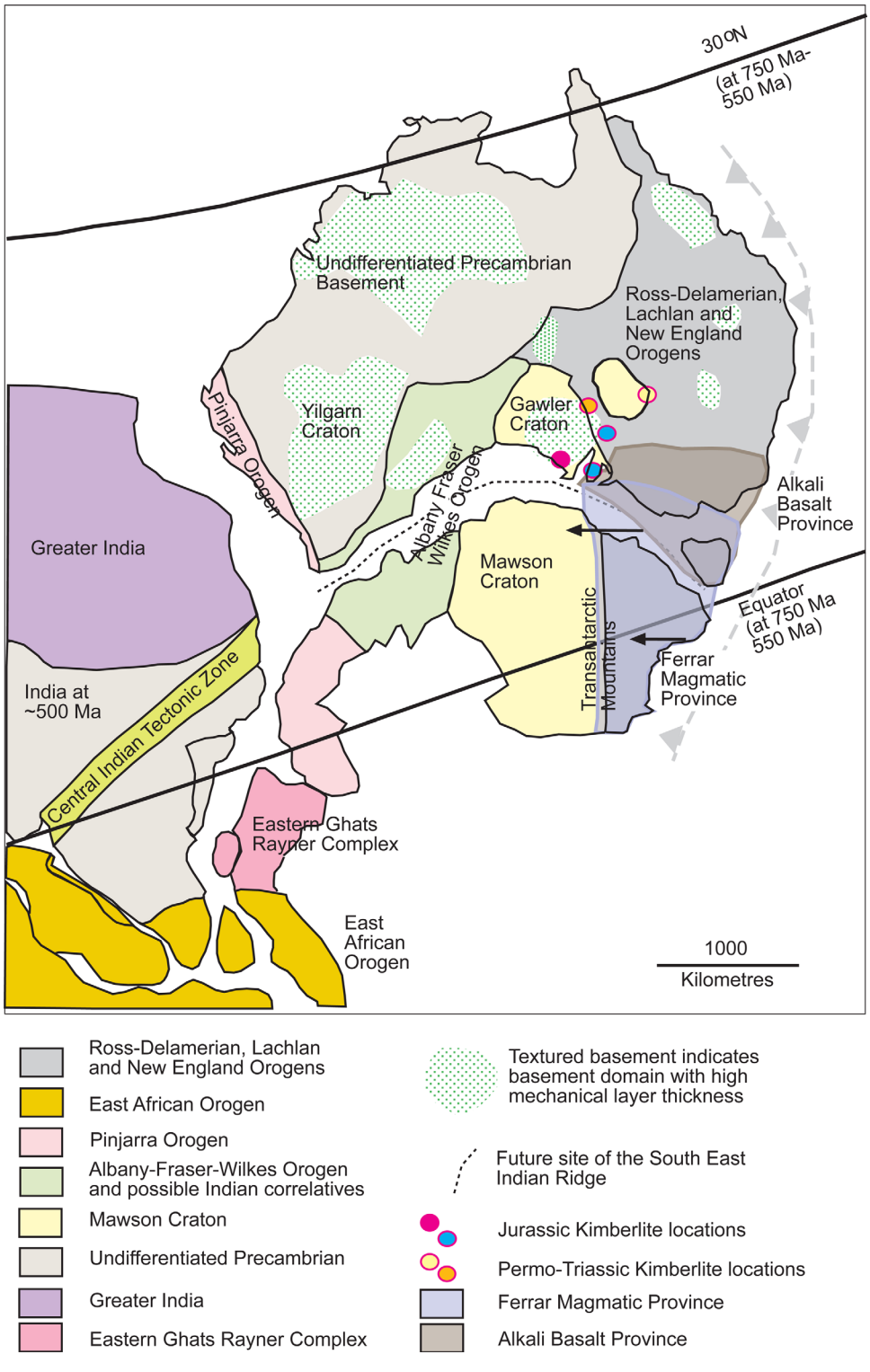

Figure 2. Cartoon reconstruction of East Gondwana at ~500 Ma (after *Fitzsimons* [2003]). In the period between ca. 550–100 Ma, eastern Gondwana was flanked by a long-lived accretionary orogeny [*Gurnis and Müller*, 2003]. The light green polygons represent the basement regions that indicate high mechanical strength [*Simons and van der Hilst*, 2002]. The approximate palaeolatitudes are after *Torsvik et al*. [2001]. Red circle: Jurassic kimberlites (180 ± 3 Ma) [*Wyatt et al*., 1994]. Blue circles: Jurassic kimberlites (170–172, 164–174 Ma) [*Ferguson et al*., 1979; *Stracke et al*., 1979]. Yellow circle: Kimberlitic pipe and dykes (260 Ma) [*Strake et al*., 1979]. Orange circle: Kimberlite (260 Ma [*Gaul et al*., 2003]. Blue area in eastern Antarctica and southern Australia: Ferrar tholeiitic basalt province (183–170 Ma) [*Hergt et al*., 1991; *Foden et al*., 2002]. Brown area in southern Australia: Alkali basalts (191 and 187 ±18 Ma) [*Hergt et al*., 1991; *Foden et al*., 2002; *Elburg and Soesoo*, 1999].

Table 1. Qualitative Comparison of Geoscience Australia Seismic Reflection Data Used to Image Upper Crustal Structure of the Southern Australian Margin[a]

Seismic Survey	Seismic Imaging of Top Basement	Seismic Record (s)	Region of Coverage
AP81	Moderate	9	Polda trough
DH91;92	Poor	6	Duntroon
HD95	Poor	6	Duntroon
DWGAB	Good	10	Ceduna
HRGAB	Variable/good	5	Ceduna
SHELL	Variable/poor	13	GAB
065	Variable/poor	13	Recherche/Eyre
S199	Excellent	15	COTZ
SA68;69	Poor	7	Ceduna
SA70W	Variable	8	SE Ceduna
S137	Good	14	Otway

[a]COTZ: Continent Ocean Transition Zone. Data classified as poor have low signal-to-noise ratio and poor depth penetration.

argued for lithospheric-scale simple shear to produce the asymmetry. *Sayers et al*. [2001] suggested on the other hand that symmetrical margins resulted from extensional deformation of rheologically layered lithosphere by pure-shear boudinage, similar to patterns in the sand-silicon model of *Brun and Beslier* [1996]. *Direen et al*. [2011] adopted aspects of both studies in arguing for the presence of symmetrical crustal detachments between an unusually strong lower crust and weak middle crust. Using the same data, *Espurt et al*. [2012] used balanced cross sections to propose a model of pure shear during initial rifting evolving to a single lithospheric-scale detachment during eventual rupture. *Direen et al*. [2012] recently argued that the margins host both symmetric and asymmetric segments. Here we adopt a 3-D approach using gravity and magnetic data to interpolate between profiles and so visualize along-strike changes that provide insights into fault-controlled and magmatic strain patterns as rifting progresses to seafloor spreading.

2. Geophysical Data Sets

2.1. Seismic Reflection Data

[11] Figure 1 locates the long-offset 2-D seismic reflection data available to this study. Seismic interpretations are based on the stratigraphic framework of *Totterdell et al*. [2000] and *Mantle et al*. [2009]. The seismic data have not been depth converted, owing to poor velocity control in deeper sections. The record length and quality of the vintage Australian seismic database was highly variable (Table 1). On the Antarctic margin, only published lines were available for comparison and are reinterpreted here in light of our results [*Colwell et al*., 2006; *Eittreim*, 1994; *Eittreim and Smith*, 1987; *Wannesson*, 1991; *Wannesson et al*., 1985]. We use products of the gravity and magnetic anomaly data to correlate crustal structures between seismic reflection profiles.

2.2. Magnetic Data

[12] Onshore Australian merged aeromagnetic data are sourced from *Petkovic and Milligan* [2002]. Offshore Australia, the data set consists of leveled ship-track data that have been merged with the onshore aeromagnetic anomalies [*Petkovic et al*., 1999a, 1999b]. Across Antarctica the Earth Magnetic Anomaly Grid 2 data set [Maus *et al*., 2009] is used. Both the Antarctic and Australian data were reduced to the pole, assuming a declination of 4.3° and inclination of −66.3°, values at the center of the study region (Figure 3). Profiles were extracted from these grids to complement the seismic sections.

2.3. Gravity Data

[13] Four separate data sets were used to produce terrain-corrected Bouguer gravity anomaly maps for the Australian margin: (1) an onshore simple Bouguer grid [*Petkovic et al*., 2001]; (2) offshore shipboard gravity data of various vintages and qualities [*Petkovic et al*., 2001]; (3) free-air gravity anomalies derived from satellite altimetry data [*Sandwell and Smith*, 1997, 2009]; and (4) a merged topographic and bathymetric data set [*Petkovic et al*., 2001]. Offshore Australia, a new merged shipboard and satellite free-air gravity grid was created from the shipboard data and the satellite data. After comparison of spectral content of the satellite and shipboard data, a 35 km cosine low-pass filter was applied to the satellite data. Datum shifts in shipboard data [*Petkovic et al*.,

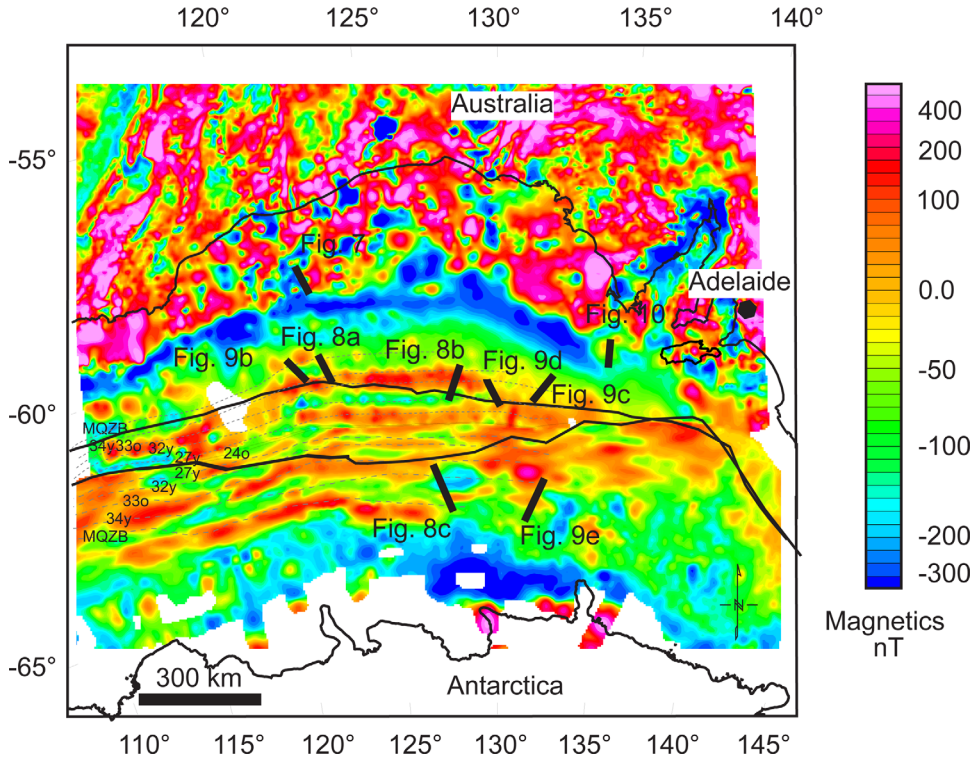

Figure 3. Reduced to pole, magnetic anomalies for Australia and Antarctica. The grids are clipped to the isochron interpretation c24o of Tikku & Cande (1999) and then rotated to the c24o (53 Ma) using the Euler pole of rotation from *Whittaker et al*. [2007]. Antarctica is held in present-day position. Antarctic data are from *Maus et al*. [2009] and they are merged with the Australian onshore-offshore data from the southern margin of Australia [*Petkovic et al*., 1999a, 1999b]. Magnetic chron interpretations, light grey dashed line (MQZB-c24o) come from *Tikku and Cande* [1999]. MQZB: Magnetic Quiet Zone Boundary: Black solid line: COB Thick black markers indicate the sector and location of the seismic line that is used in the respective figures. Projection: Universal Polar Stereographic (median longitude 130°E)

2001] were corrected via cross-over analyses, and then draped on the longer wavelength satellite gravity field. This process improved the root-mean-square misfit between the ship track and filtered satellite data from ±18.7 to ±9.9 mGal.

[14] On the Antarctic margin, this study uses only the satellite derived [*Sandwell and Smith*, 1997, 2009] data. After testing of the satellite signal-to-noise ratio, a 35 km cosine low-pass filter was applied to the satellite data in order to reduce their characteristic "orange peel" noise [e.g., *Sandwell and Smith*, 1997; *McAdoo and Laxon*, 1997].

[15] After gridding these data, simple Bouguer anomalies were calculated by assuming a water-rock density difference of 1670 kg m^{-3} to facilitate merger with the land data (Figure 4a). This produces a more positive anomaly than in other offshore studies because the mean density contrast between offshore sediments and water is 1300–1400 kg m^{-3} [e.g., *Close et al*., 2009]. Owing to the large variations in water depth, terrain corrections were applied on the basis of the topographic data set [C. Deplus, personal communication 2002]. Minor artifacts at the seam between the merged onshore and offshore Bouguer grids are probably the result of bathymetric variations for which no terrain correction was applied to the land-based Bouguer gravity. The merged onshore-offshore data are gridded at 4 km spacing.

3. Analyses

3.1. Gravity Data Analyses

[16] Before interpreting the gravity data set, we filtered wavelengths longer than 60 km associated with deep Earth structure. We then computed the tilt derivative as an edge detector to locate density variations within the crust and uppermost mantle, and to calibrate these locations with independent data [e.g., *Cooper and Cowan*, 2006; *Salem et al*., 2008] (Figure 4b). The tilt derivative method uses

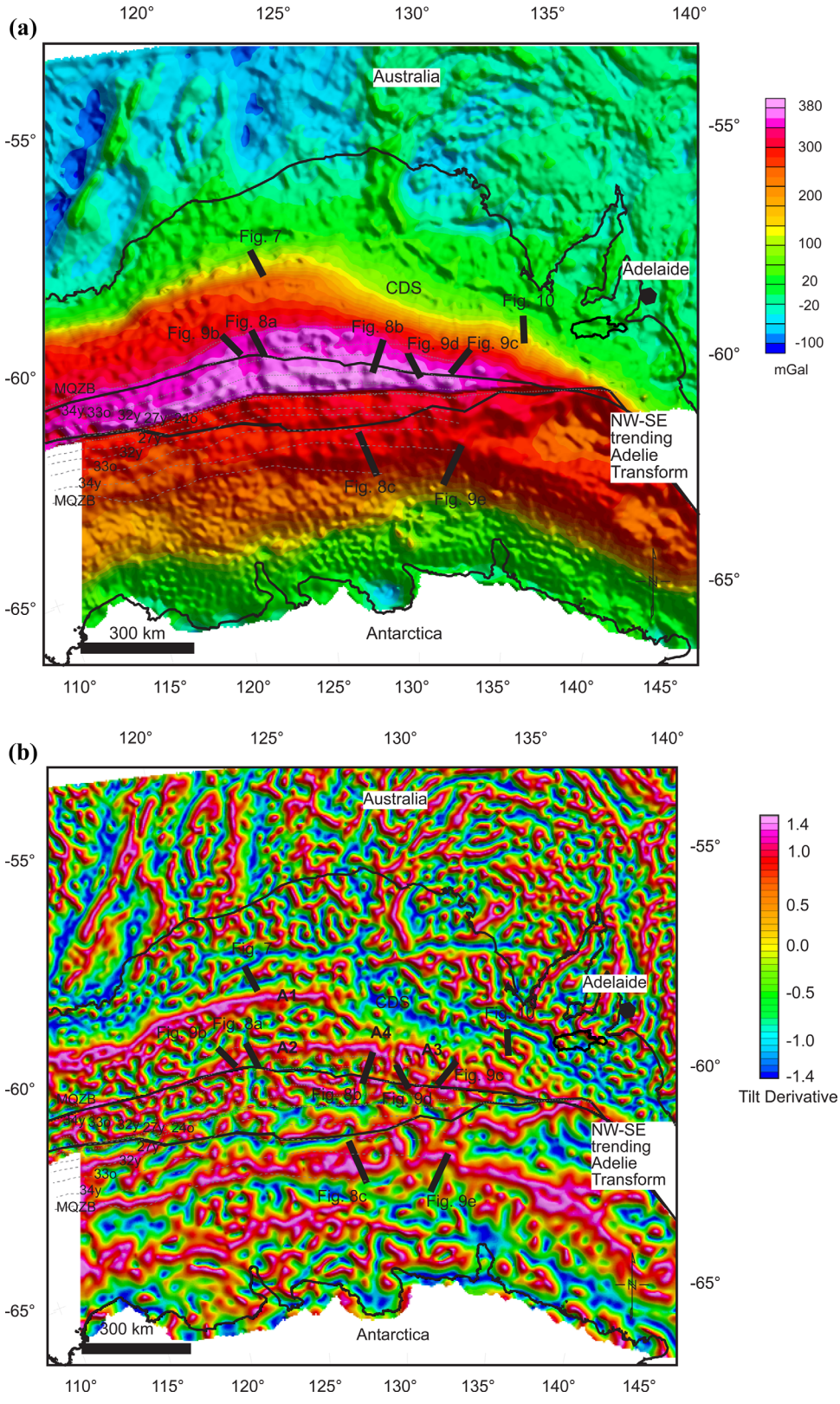

Figure 4. (a) Bouguer gravity anomaly; (b) Tilt derivative of the Bouguer gravity, in radians ($-\pi/2$ to $\pi/2$); (c) Solutions from the Euler 3-D deconvolution of the Bouguer gravity. Structural index SI = 0.0 representing a small fault or step. Within Figure 4b the seismically defined border faults: black lines: Phase 1 border faults; orange lines Phase 2 border faults. The Australian Euler solutions and tilt derivative grids are rotated to the c24o (53 Ma) using the Euler pole of rotation from *Whittaker et al*. [2007]. Plate reconstructions as for Figure 3. Magnetic chron interpretations, light grey dashed line (MQZB-c24o) come from *Tikku and Cande* [1999]. MQZB: Magnetic Quiet Zone Boundary: Black solid line: COB. Thick black markers indicate the sector and location of the seismic line that is used in the respective figures.

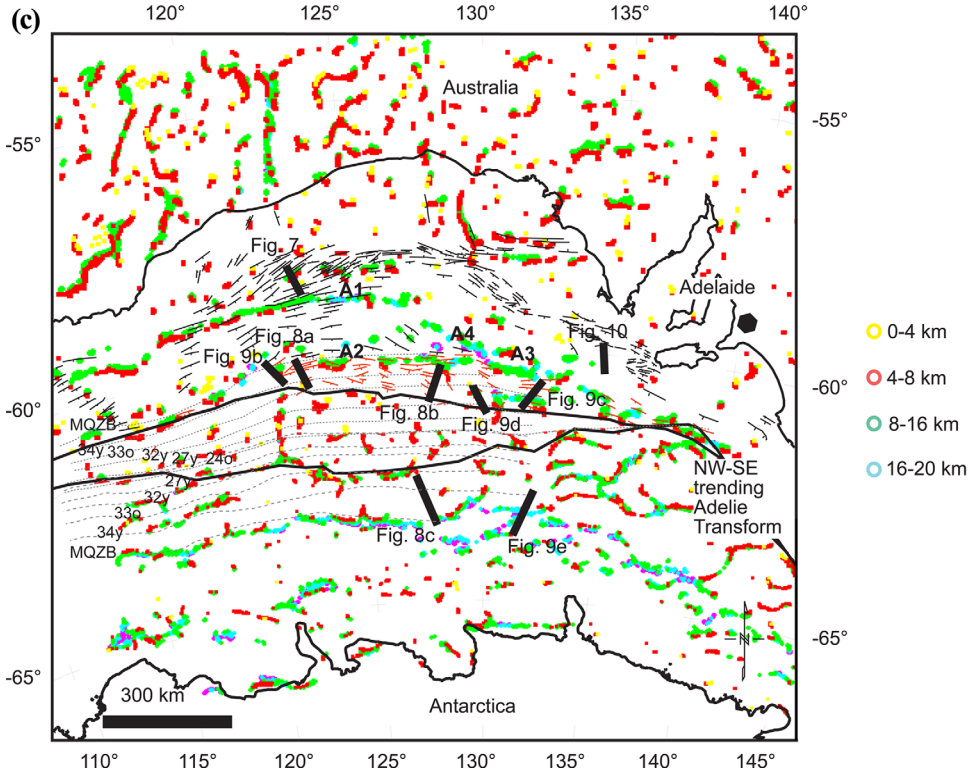

Figure 4. (Continued).

second derivatives to delineate the depth and position of source bodies, without requiring assumptions about the shapes of subsurface bodies. We also used Euler deconvolution (Figure 4c) to locate the boundaries of causative bodies for the observed anomalies [e.g., *Reid et al*., 1990]. This inverse method requires assumptions about the shapes of causative bodies, which will determine the rate of change of the gravity or magnetic field with distance. We iterate through a range of shapes represented by structural indices and invert for position [e.g., *Reid et al*., 1990; *Marson and Klingele*, 1993; *Stavrev*, 1997]. Visual inspection is used to evaluate the appropriateness of a particular structural index for a particular subsurface body, as outlined in *Reid et al*. [1990]. We used a window size of 40 km × 40 km to ensure an overconstrained problem, and to focus results on basement-involved structures.

[17] The terrain-corrected Bouguer anomaly was inverted to constrain Moho topography using the iterative procedures of *Parker* [1972] and *Oldenburg* [1974]. The inversion is sensitive to two free parameters; (1) the assumed density contrast at the crust/mantle interface; and (2) the a priori reference level about which the calculated Moho topography is assumed to vary within the area of investigation [e.g., *Tiberi et al*., 2005]. In the absence of calibrated sediment thickness and density maps for the conjugate margin regions, we use the complete Bouguer anomaly values, and discuss potential biases below. We first filtered the data to remove anomalies associated with shallow and sublithospheric density variations ($<95\,\lambda>$ 190 km), including the poorly mapped sediment thickness, and mirrored data. Residuals between observed and predicted anomalies were <1 mGal along the Australian margin, and <0.8 mGal along the Antarctic margin.

[18] A density contrast of 480 kg m^{-3} was assumed for the crust/mantle interface, corresponding to crust and mantle densities of 2670 and 3150 kg m^{-3}. Within the range 400–550 kg m^{-3}, this 480 kg m^{-3} contrast provided the best fit to seismic estimates of crustal thickness near the ocean-continent boundary. We adopt a reference crustal thickness of 25 km across the Australian margin, taking into account the ~40 km crustal thicknesses observed onshore from refraction studies [e.g., *Clitheroe et al*., 2000]. A reference value of 15 km was used on the Antarctic margin in view of thinner crust recorded there; this in turn

suggests that the gravity data coverage across the Antarctic margin is limited by the ice shelf to more distal parts of the margin. Synthetic models indicate that variations of 5 km in the reference depth lead to differences in crustal thickness of ~2 km [*Tiberi et al*., 2001].

[19] Several factors lead to local bias in the crustal thickness estimates. We have assumed a uniform Bouguer slab density of 2670 kg m^3 throughout the onshore and offshore regions. Gravity anomalies over rock layers with densities differing from this assumption will have introduced spurious crustal thickness variations to our grids. For example, in areas of the shelf with thick sedimentary layers, the Bouguer correction density exceeds the real density of the sedimentary layers between the seabottom and stretched basement. The high-cut filter partially accounts for this, but crustal thickness estimates offshore may still be anomalously thick, relative to those in the onshore regions.

[20] Without making assumptions regarding layer density, we can estimate crustal thickness variations by subtracting the thickness of sedimentary and water layers, using a model constrained by seismic reflection data. On the Australian margin, sedimentary layer thicknesses were calculated from the seismic reflection data using the velocity model of *Petkovic* [2004], which has an estimated velocity error of ≤15%, increasing with depth. Our sediment thickness estimates match within 2% of data from sparse wells, suggesting that thickness is known to ~3000 m in the most thickly sedimented regions of the Ceduna Delta region. Along the Antarctic margin, we adopt the minimum sediment thickness model of *Williams et al*. [2011]. Where seismic reflection data is lacking along the Antarctic margin, the maps were supplemented using the global sediment compilation of *Laske and Masters* [1997].

4. Results

4.1. Tilt Derivative and Euler Deconvolution

[21] The results of the tilt derivative and Euler Deconvolution procedures are shown in Figures 4b and 4c. Onshore in Australia, the tilt derivative shows patterns of variability consistent with the known presence of regions of strong crustal heterogeneity. Trends in both the tilt derivative and Euler solutions reproduce the strikes of boundaries between these regions. Offshore distinct tilt derivative anomalies and clustered Euler solutions are observed and several distinct trends are enhanced. These anomalies and solutions are therefore a viable basis for interpolation of regional structures between the seismic reflection interpretations. These will be further discussed below and interpreted in conjunction with the seismic observations.

4.2. Moho Inversions

[22] The results of the inversion for crustal thickness minus water layer and sedimentary layer thicknesses are shown in Figure 5a. The spatial pattern of crustal thickness variations matches well with onshore and offshore seismic refraction and wide-angle reflection data, and receiver function data. Our results match within ±2 km oceanward of the shelf break; misfits are as much as 5 km in the area of the shelf break where the gravity gradient is greatest. Owing to the assumption of uniform crustal density in the inversion for Moho topography, lateral density variations will appear as crustal thickness variations, consistent with the largest discrepancy between predicted and observed beneath the edge-effect anomaly zone.

4.3. Crustal Stretching Factor

[23] We use the water and sediment-corrected, predictive map of crustal thickness to estimate crustal stretching factors, assuming a uniform prerift crustal thickness of 40 km along the length of the Great Australian Bight (Figure 5b). This prerift thickness was chosen using the limited seismic refraction database from the onshore regions of the Australian and Antarctic margins, and like the Moho depth estimates are subject to caveats regarding lateral density variations within the crust across the conjugate margins. Previous studies [*Brown et al*, 2003; *Hegarty et al*., 1988] assumed thinner prerift crustal thicknesses and thus present smaller stretching factors.

[24] Crustal stretching is estimated at $\beta < 1.4$ across the shallow shelf, with values increasing sharply to $\beta > 4$ in the deepwater margin region. The contour map suggests distinct sectors with greater stretching, most notably the continental rise south of the Ceduna Delta System (Figure 5b). We overlay these models of stretching with interpretations derived from analyses of 2-D seismic reflection profiles and the Euler deconvolution and tilt-derivative products in Figure 5b, and integrate them below.

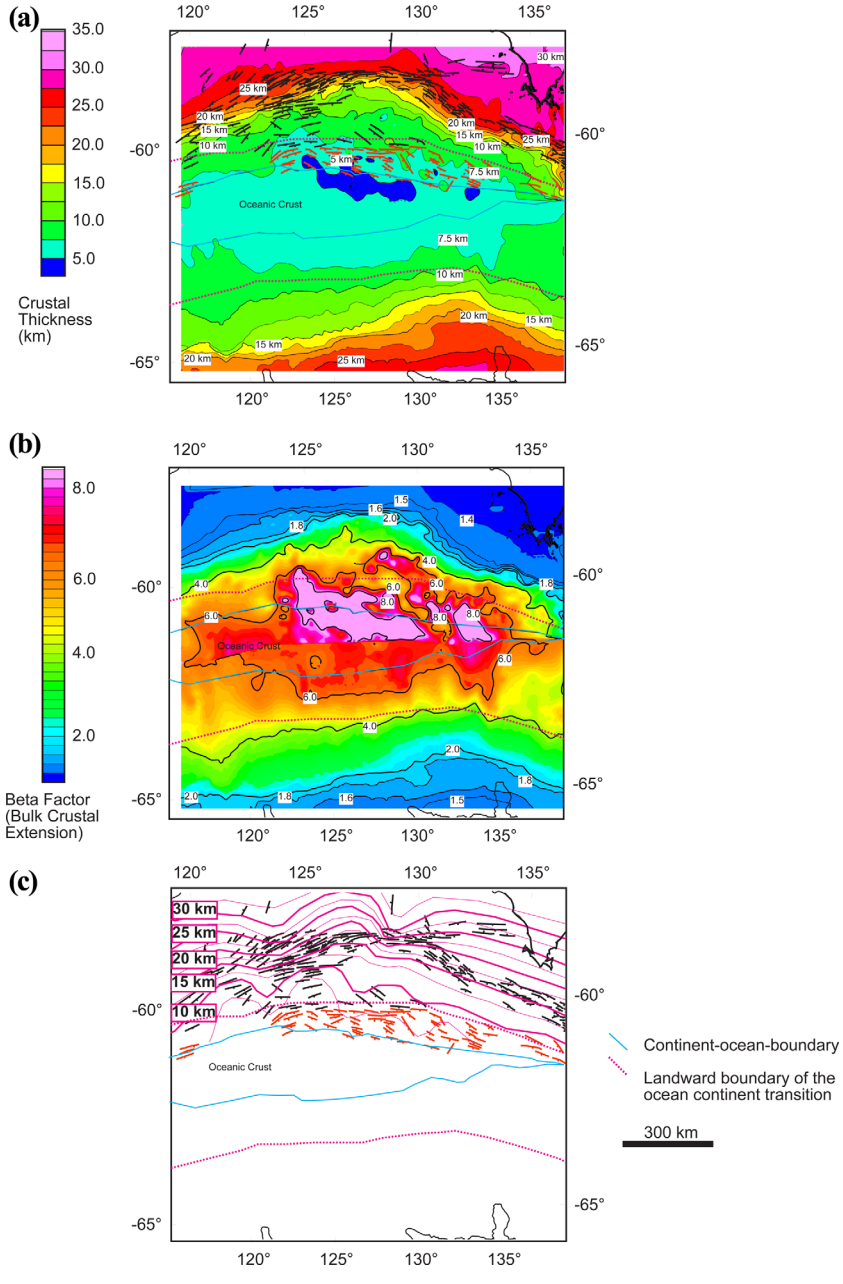

Figure 5. Crustal thickness grids for Australia and Antarctica. Plate reconstructions as for Figure 3. (a) Crustal thickness grid for Australia and Antarctica (this study see text). Moho depths from sonobuoy and seismic refraction experiments on the Australian and Antarctic margins range between 11.5 and 26.5 km [e.g., *Hawkins et al*., 1965; *Konig and Talwani*, 1977; *Talwani et al*., 1978; *Konig*, 1987; *Childs and Stagg*, 1987; *Clitheroe et al*., 2000; *Stagg et al*., 2005], (b) stretching factors computed from the crustal thickness grids in Figure 5a. Prerift crustal thickness is assumed to be 40 km. (c) The red contours are crustal thickness contours after *Brown et al*. [2003]. Basement faults identified from seismic reflection data and possible mafic bodies are overlain to examine the distribution of faulting and crustal thickness. This is done to establish where the border faults of rift Phase 1 (black fault traces) and rift Phase 2 (orange fault traces) are located in relationship to the crustal thickness establishing a spatial relationship between bulk crustal thinning and observed basement faults.

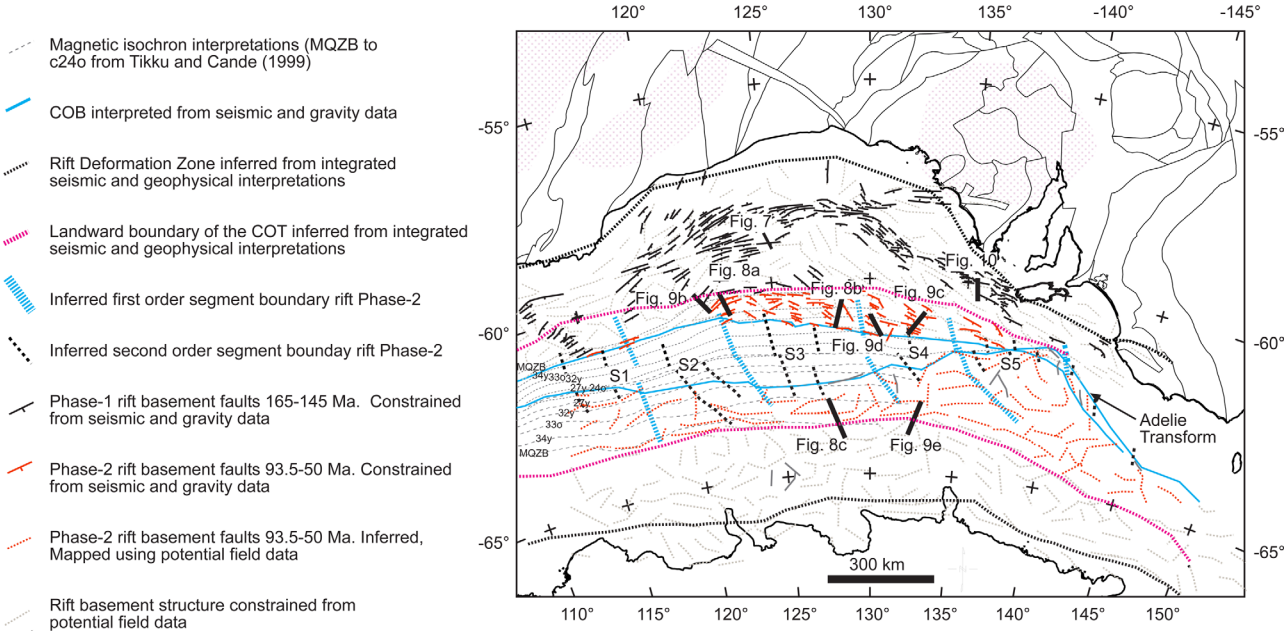

Figure 6. Basement fault map interpretation based on seismic reflection data. Fault traces are simplified for simplicity. Black fault traces are interpreted to have a 165–145 Ma age. Orange fault traces are identified to be younger with ages between 93.5 and 50 Ma. Plate reconstruction as for Figure 3. Onshore crustal elements after *Shaw et al.* [1996]. Magnetic chron interpretations, light grey dashed line (MQZB-c24o) come from *Tikku and Cande* [1999]. MQZB: Magnetic Quiet Zone Boundary.

4.4. Basement-Involved Faults and Structures of the Bight Basin

[25] Age constraints on the timing of fault movements and basin subsidence are derived from interpretation of seismic tectonostratigraphic sequences. Stratigraphic interpretations use the supersequences described by *Totterdell et al.* [2000] and *Mantle et al.* [2009] and were tied to the available exploration well database, which is largely restricted to the half-graben basins along the shelf (Figure 1). Large offset (>500 ms) basement-involved faults were mapped along profiles and then tied to features in the tilt derivative and Euler deconvolution results to determine their lateral extent (Figure 5). Numerous large syn-sedimentary listric faults within the Ceduna sub-basin detach on a regional surface within the Blue Whale supersequence and are not directly interpretable in terms of lithospheric stretching. We omit them from our considerations.

[26] The stratigraphic interpretations provide important temporal constraints on the interpreted faults. From this process, Figure 6 shows it is possible to distinguish two distinct phases of basement-involved faulting that formed two distinct populations of faults. The hanging walls of Phase 1 faults (black lines) are characterized by syn-rift "wedge-shaped" thickening of the Sea Lion and Minke supersequences (165–145 Ma). The hanging walls of Phase 2 faults (orange lines) show thickening of the Tiger, Hammerhead and Wobbegong supersequences (93.5–50 Ma). Within the proximal parts of the margin, we do not observe widespread or significant reactivation of the Phase 1 basement faults during the deposition of the Tiger-Hammerhead or Wobbegong sequences. It seems therefore that at this time strain came to be accommodated within a narrow more distal region populated by new, Phase 2, faults (Figure 6). Consistent spatial and temporal patterns are summarized in more detail below.

4.4.1. Phase 1: 165–145 Ma

[27] Phase 1 structures largely form simple half-grabens, bordered by planar normal faults. The seismic defined faults have observed throws greater than 500 ms Two-Way Time (TWT), with dominant south east or south-south east dips that are filled by wedge-shaped reflectors. Minimal or no footwall uplift is preserved, and across the shelf-edge younger sequences are noticeably condensed and often eroded (Figure 7). Basins of this

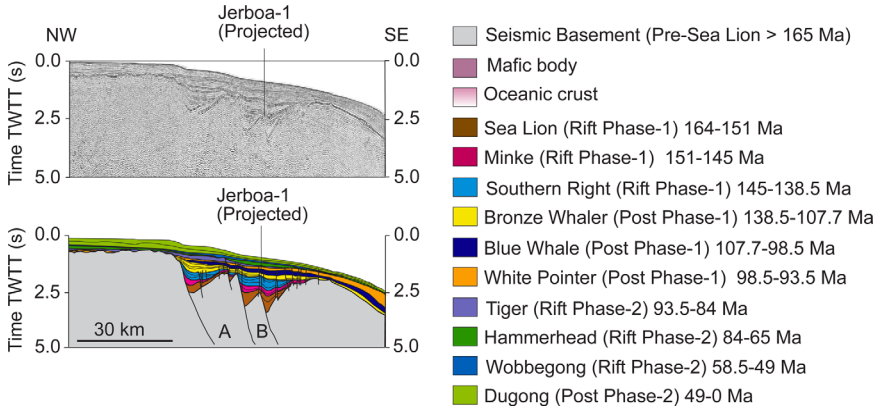

Figure 7. Phase 1 rift basins: seismic line 199-09 shows an example of the half graben structures from the Eyre Sub-basin, typical of the phase 1 rift structures (165 to ~145 Ma). Exploration well Jerboa-1 has been used to tie the seismic interpretation. It is projected onto the seismic line by ~20 km. The stratigraphic interpretation is derived from *Totterdell et al*. [2000], modified by *Mantle et al*. [2009]. This 2-D seismic profile is located at a right angle to the strike of the border fault. The basin [A] is 15 km wide and the estimated basin syn-rift fill is approximately 1 s (TWT). The basin [B] is 20 km wide and is characterized by a syn-rift fill of 1.25 s (TWT). For the location of the seismic images see Figure 6. The seismic image used in this figure is published with permission from Fugro MCS.

phase are overlain by thin postrift sequences on the shelf, and there is no evidence for syn-rift or postrift magmatism. The best examples occur on the shelf and just basinward of the present-day shelf edge in the Bremer, Eyre, and Duntroon subbasins of the Australian margin (Figure 7). Similar half-grabens can be interpreted basinward of this, but only on seismic profiles with >10 s TWT records, due to the increase in water depth and increasing thickness of the sedimentary cover. Where identified, these deeper basins cannot confidently be correlated along strike using gravity anomalies, and their age cannot be accurately constrained. The border faults accommodate dominantly down-to-the-south movements and roughly correspond with W-E gravity and magnetic anomalies (A1) between 120°E and 130°E (Figures 3–5). East of 130°E, within the Ceduna subbasin and northern Otway Basin, the orientation of the shelf edge changes to NW-SE. The shelf-edge gravity anomaly decreases in amplitude owing to the thick (~15.3 km) sedimentary pile of the Ceduna Delta System (Figures 1 and 4b). Seismic interpretation reveals scarcely any basement faults north of the Phase 1 faults along the Gawler shelf. This abrupt partitioning of strain is also seen in crustal thickness patterns (Figure 5a), and is thought to coincide with the edge of the present-day Archaean-Mesoproterozoic Gawler Craton [*Totterdell et al*., 2003].

[28] The crustal thickness and bulk crustal thinning maps reveal that Phase 1 faults occur in slightly stretched (β < 1.3–2.0) crust ~50 km landward of a sharp reduction in crustal thickness (Figures 5a and 5c). These stretching factors exceed the thinning that can be estimated from upper crustal fault displacements, indicating depth-dependent stretching and/or inadequate seismic resolution of crustal strains.

4.4.2. Phase 2: 93.5–50 Ma

[29] For the most part, Phase 2 structures are products of localized extension on new basement faults that formed after the cessation of slip along Phase 1 faults. In some areas, Phase 1 sedimentary sequences are deformed by Phase 2 fault rotations (e.g., Figures 8a and 8c). Evidence for repeated episodes of cannibalization of Phase 2 rift basins can be interpreted in some rift sectors, becoming more common eastward and basinward in the Phase 2 rift [*Sayers et al*., 2001] (Figure 8b). This phenomenon of discrete overlapping has been documented along other rifted margins [*Roberts et al*., 1999; *Péron-Pinvidic et al*., 2007]. The sequential deformation that is observed within the Phase 2 rift (Figures 8a–8c) may suggest that the localization represents a new phase of deformation, after strain hardening embrittled the crust, allowing new faults to accommodate ongoing strain [e.g., *Ranero and Pérez-Gussinyé*, 2010].

[30] Within the deepwater parts of the Australian and Antarctic margins, potential field anomalies are of too coarse a resolution to extend individual fault interpretations through the study region (Figures 3, 4, and 6). The laterally continuous anomaly (A2) and associated E-W trending Euler

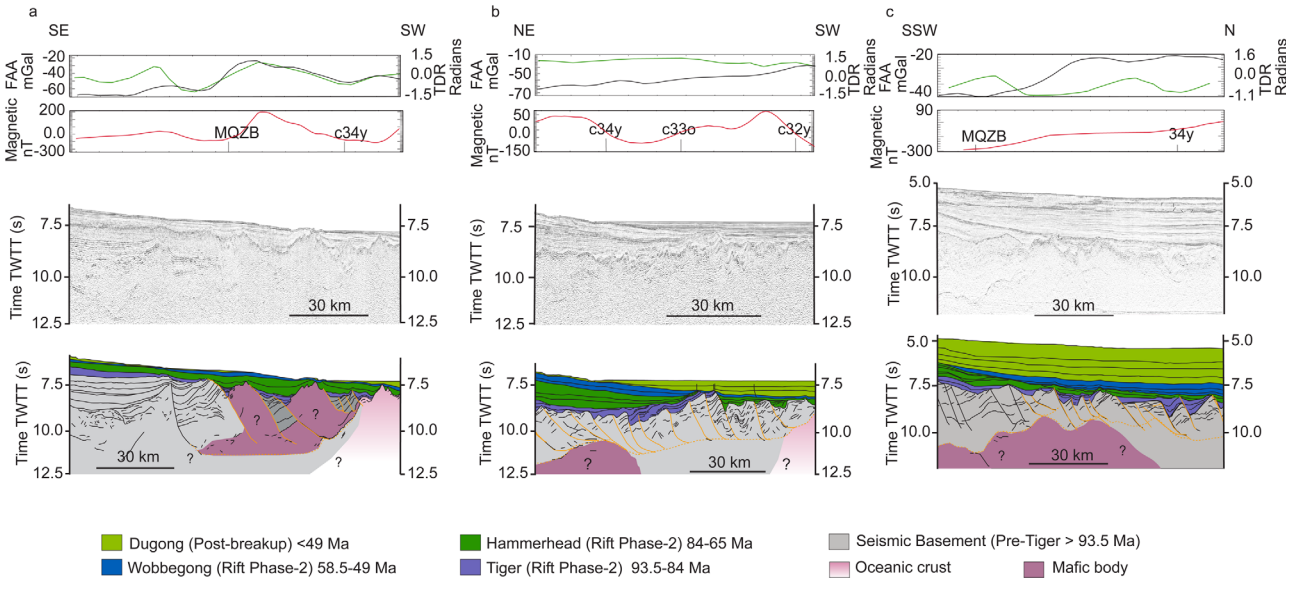

Figure 8. Phase 2 rift basins structural style and overprint of older Rift Phase 1 basins. The observation of oceanward migration of tectonic activity and structural overprinting of interpreted Rift Phase 1 basins suggests that there was a reorganization of strain prior to breakup. (a) Seismic profile: 199-01, (b) seismic profile: 199-07, (c) seismic profile: 228/24, modified from *Colwell et al*. [2006]. Each seismic example is accompanied by profiles: Free-Air gravity anomalies (black); tilt derivative (green) and Reduced to the Pole magnetic anomalies (red). As in Figure 6 the Phase 1 faults are marked in black (165–145 Ma) and the Phase 2 faults in orange (93.5–50 Ma). For the location of the seismic images see Figure 6. Magnetic chron interpretations, (MQZB-c24o) come from *Tikku and Cande* [1999]. MQZB: Magnetic Quiet Zone Boundary. Figure 8 displays only a part of the complete seismic line and interpretation. Full line figures with interpretations are available as supporting information.[1] Lines 199-01 and 199-07 are published with the permission of Fugro MCS. The line 288/24 is from the GA228-24 (Australian Survey 2001), available via http://www.scar-sdls.org, the principal Antarctic library for seismic data.

deconvolution results correlate spatially with our Phase 2 rift zone interpreted from Phase 2 faults in seismic reflection data (Figures 3–5). Where seismic data are lacking, we interpret (A3) as the landward boundary of Phase 2 rift structures under the Ceduna Delta System (A3, Figure 4).

[31] The Phase 2 faults are more variable than those of Phase 1. Steep and highly rotated stratal dips are observed (Figure 8). The faults that show the greatest throw are of Tiger (93.5–84 Ma) to early Hammerhead (83.5–65 Ma) age; the largest of these exhibit footwall uplift (Figure 9). Compared to Phase 1 relationships, the postrift sequence is thinner (1–2 km), displacements on the faults are smaller so that the syn-rift topography is flatter, and the faults are more closely spaced (Figures 9a–9c). Phase 2 faults are dominantly planar and appear to sole out at the Moho or lower crustal detachments (e.g., Figure 8b). This style of faulting implies extension of weaker crust compared to that in which the Phase 1 border faults developed. Stretching factors in the Phase 2 rift are typically $\beta > 5$ (Figures 5b and 5c). Consistent with this, our crustal thickness grid, like those of *Brown et al*. [2003] and *Kusznir* [2009], shows that the Phase 2 faults are all located within crust that is <7.5 km thick (Figures 5a and 5c).

[32] Phase 2 structures lie seaward of a ~50–100 km wide zone just basinward of the shelf edge over which the crustal thickness changes from >25 to <15 km (Figure 5a). The recognition that Phase 2 faults are spatially segregated into a region of thinner crust implies an important change in the evolution of the Australian-Antarctic rift. This change might be attributed to crustal stretching that accompanied or postdated the development of Phase 1 faults at 165–140 Ma, but is challenged by the discrepancy between the stretching accommodated by total crustal thinning

[1]Additional supporting information may be found in the online version of this article.

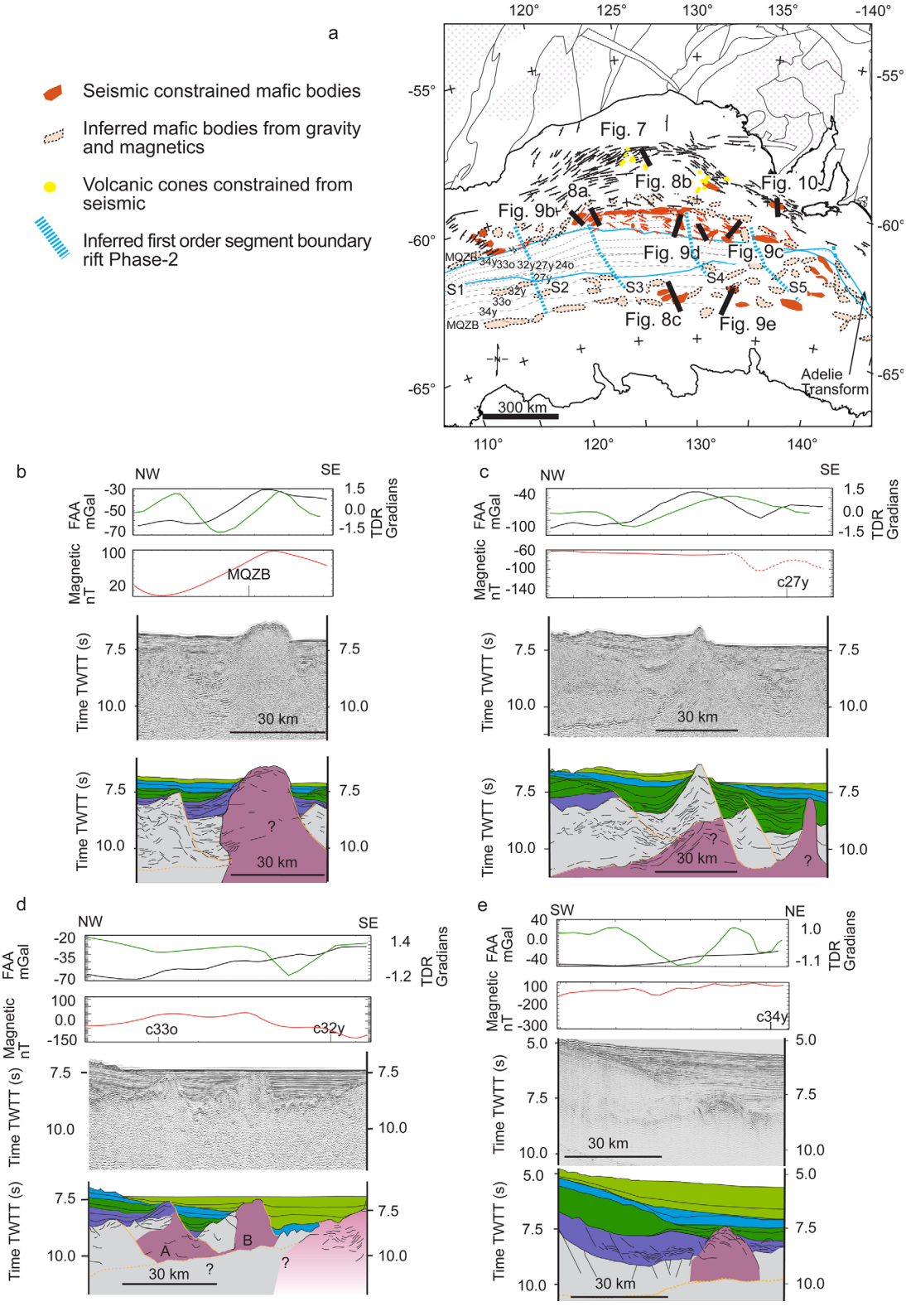
a
Seismic constrained mafic bodies
Inferred mafic bodies from gravity and magnetics
Volcanic cones constrained from seismic
Inferred first order segment boundary rift Phase-2
120°
125°
130°
135°
-140°
-55°
-60°
-65°
110°
120°
130°
140°
Fig. 7
Fig. 8a
Fig. 8b
Fig. 8c
Fig. 9b
Fig. 9c
Fig. 9d
Fig. 9e
Fig. 10
MQZB
S1
S2
S3
S4
S5
Adelie Transform
300 km
b
c
d
e
NW
SE
SW
NE
FAA mGal
TDR Gradians
Magnetic nT
Time TWTT (s)
MQZB
c27y
c33o
c32y
c34y
30 km
A
B
?

Figure 9.

Table 2. Geometry of the Margin Determined Within Various Plate Kinematics and Geophysical Studies of the COTZs in Five Identified Rift Phase 2 Segments (S1–S5, Figure 7)[a]

Model/ Region Reviewed	S1	S2	S3	S4	S5
Width of margin (including COTZ)					
This study: Australia	280	300–370	400–440	400–450	130–300
This study: Antarctica	410–420	410	350–380	390–400	450–520
Direen et al. [2012]: Australia	330	340–370	430–440	420–450	250–320
Direen et al. [2012]: Antarctica	450–480	440–500	360–420	410–440	470–530
Williams et al. [2011]: Australia	230–270	260–340	320–340	320–350	130–300
Williams et al. [2011]: Antarctica	230–260	290–300	250–270	320–350	400–480
Whittaker et al. [2013]: Australia	250–270	280–320	340–350	370–430	140–300
Whittaker et al. [2013]: Antarctica	170–250	250–270	200–220	220–260	300–350
Width of COTZ (km)					
This study: Australia	50–70	70–90	100–120	130	30–80
This study: Antarctica	150–200	120–140	110–120	150–170	220–310
Direen et al. [2012]: Australia	60	60–90	80–100	15–90	30–120
Direen et al. [2012]: Antarctica	180–240	110–150	80–100	80–100	70–80
Length of segment (along axis) (km)					
This study: Australia	330	270	420	210	345
This study: Antarctica	<240	260	330	250	350
Direen et al. [2012]: Australia	n/a	n/a	n/a	n/a	n/a
Direen et al. [2012]: Antarctica	n/a	n/a	n/a	n/a	n/a

[a]The ranges in the numbers represent the min-max width measured within the Margin or COTZ.

and the stretching accommodated on these faults and faults within the zone of maximum crustal thickness change. Alternatively, or additionally, 1-D pseudowell analysis has revealed sediment accumulation in the period 110–100 Ma [*Totterdell et al*., 2000; *Brown, et al*., 2001], which might be attributed to ongoing or renewed stretching related to the onset of the new Phase 2 rift. Existing seismic data are not adequate to constrain a possible diachronous start to this rifting episode, nor can they differentiate between a range of models that might account for the discrepant stretching estimates [e.g., *Totterdell et al*., 2000; *Totterdell and Bradshaw*, 2004; *Brown et al*., 2001; *Gurnis et al*., 1998; *Brown et al*., 2001; *Gurnis and Müller*, 2003; *Angelo*, 2011; *Williams et al*., 2011].

5. Integrative Interpretations

5.1. Continent Ocean Transition and Continent Ocean Boundary

[33] For the following, we define the continent-ocean transition zone (COTZ) as a region of laterally variable crustal composition and density structure, across which either a large volume of igneous material has been intruded, or where stretched continental crust is juxtaposed to lower crustal rocks, exhumed continental mantle peridotites, and/or mafic igneous rocks (Figure 6). This zone therefore forms the transition between crustal zones of continental and oceanic affinity. The continent-ocean boundary (COB) presented here is a simplified tectonic line that delineates the

Figure 9. (a) Interpreted mafic bodies from the Australian and Antarctic margins, and (b–e) line locations for the seismic images. The interpretations are rotated to the c24o (53 Ma) using the Euler pole of rotation from *Whittaker et al*. [2007]. Plate reconstructions as for Figure 3. Onshore crustal elements after *Shaw et al*. [1996]. Magnetic chron interpretations, light grey dashed line within, Figure 9a, (MQZB-c24o) come from *Tikku and Cande* [1999]. MQZB: Magnetic Quiet Zone Boundary. Figure 9b seismic profile: N404-1. Figure 9c seismic profile: N407-5, Figure 9d seismic profile: 199-11, Figure 9e seismic profile: L184AN-03, modified from *Eittreim et al*. [1985]. Each seismic example is accompanied by three profiles: Free-Air gravity anomalies (black); tilt derivative (green); and Reduced to the Pole magnetic anomalies (red). The seismic example Figure 9c has a combination of magnetic anomalies from *Maus et al*. [2009] (dashed) and *Petkovic et al*. [1999a, 1999b] (solid). As in Figure 6 the Phase 1 faults are marked in black (165–145 Ma) and the Phase 2 faults in orange (93.5–50 Ma). See Figure 9a for the location of the lines. Figure 9 displays only a part of the complete seismic line and interpretation. Full line figures with interpretations are available online as supporting information. Lines N404-1, N407-5, 199-11 are published with the permission of Fugro MCS. The line L184AN-03 is from the U.S. Geological Survey, Geophysical Survey L-1-84-AN (L184AN), available from National Geophysical Data Center, NESDIS, NOAA, http://maps.ngdc.noaa.gov/viewers/geophysics.

Table 3. Kinematics of the Margin Determined Within Various Plate Kinematic and Geophysical Studies of the COTZs in Five Identified Rift Phase 2 Segments (S1–S5, Figure 7)

Model/Region Reviewed	S1	S2	S3	S4	S5
Age of breakup (Ma)					
This study—*Whittaker et al*. [2013] kinematic plate model	79–69	81–79	83–80	79–63	63–51
This study—*Williams et al*. [2011] kinematic plate model	79–69	81–79	83–80	79–63	63–51
Direen et al. [2012]: *Whittaker et al*. [2013] kinematic plate model	56–54	78–61	82–78	78–61	56–44
Direen et al. [2012]: *Williams et al*. [2011] kinematic plate model	56–54	78–61	82–78	78–61	56–44
Williams et al. [2011]	100–95	100–96	112–95	95–93	80–54
Whitaker et al. [2013]	90–88	92–89	95–92	90–83	83–80
COTZ formation age					
This study—*Whittaker et al*. [2013] kinematic plate model	93–79	90–80	95–83	100–79	105–65
This study—*Williams et al*. [2011] kinematic plate model	105–79	110–80	110–83	118–79	122–65
Direen et al. [2012]: *Whittaker et al*. [2013] kinematic plate model	86–56	86–78	91–82	88–78	83–56
Direen et al. [2012]: *Williams et al*. [2011] kinematic plate model	100–56	100–78	103–82	96–78	82–56
Estimated COTZ extension rate (mm/yr)					
This study—*Whittaker et al*. [2013] kinematic plate model	16.79	21.00	18.30	13.80	7.50
This study—*Williams et al*. [2011] kinematic plate model	9.40	10.50	7.33	7.25	5.00
Direen et al. [2012]: *Whittaker et al*. [2013] kinematic plate model	9.00	25.60	20.00	14.00	5.56
Direen et al. [2012]: *Williams et al*. [2011] kinematic plate model	10.80	10.25	6.00	3.50	2.50

landward edge of unequivocal oceanic crust, defined by high-seismic reflectivity, irregular basement with isolated seamounts, unfaulted postrift sedimentary strata, and identifiable magnetic anomalies [e.g., *d'Acremont et al*., 2005; *Autin et al*., 2010]. In the sometimes large gaps between seismic profiles, we use the gravity data products to identify mafic crust, buried seamounts, and segment boundaries (Figures 3–5).

[34] Recently published COB and plate reconstruction models differ in part owing to the key observations and assumptions used to define the first ocean crust [*Direen et al*, 2012; *Williams et al*., 2011; *Whittaker et al*., 2013]. These differences lead to distinct differences in the interpretations of rates and timing of rifting and rupture, as well as basin subsidence history, which we summarize for the cited studies and compare to our new results in Tables 2 and 3. For these tables, we measured the total margin width based on identifications of a rift deformation zone (RDZ), which is defined by observations of basement-involved faults with stratigraphic evidence for rift-related extension (Table 2) and alternatively using mapped landward boundaries and COBs in our study and that of *Direen et al*. [2012]. Owing to the presence of the Antarctic ice shelf, it is only possible to give minimum widths on that margin. Table 2 summarizes the along-strike length of the five studied margin segments. The major boundaries that define these segments are interpreted using a combination of observations from the tilt derivative grids (Figure 4b) and Euler solutions (Figure 4c) following our regional interpretations of the seismic data and the calibrated potential field data. Segment boundaries were determined based on (i) consistent changes in the orientation of interpreted faults and or mafic bodies; (ii) the interpretation of any strong obliquely trending anomalies or the lateral termination of anomalies and (iii) discrete changes in the texture of the gravity anomalies.

[35] Table 3 makes use of simple geometric fits of the COBs in this study and that of *Direen et al*. [2012] when rotating within the plate kinematic schemes of *Williams et al*. [2011] and *Whittaker et al*. [2013], in order to derive estimates of breakup ages, duration of COTZ extension and extension rates for the two COTZs. To do this, we assumed overlap of the COBs to indicate extension within the COTZ, and underlap to indicate separation of the COBs by seafloor spreading processes.

[36] *Direen et al.*'s [2012] COB and COTZ interpretation is based largely on interpretation of conjugate margin profiles, using similar criteria as described above. Plate kinematic models define a COTZ less explicitly, on the basis of their identifications of coherent magnetic anomalies that are taken to mark the onset of seafloor spreading and the landward edge of oceanic crust. However, in the *Williams et al*. [2011] model, the crust interpreted as exhumed lithospheric mantle or magmatic intrusives is considered "new crust", rather than part of a COTZ. Consequently, when comparing the width of the total margin constrained by the limit of rifting marked by the RDZ (Figure 6) the margin widths of *Direen et al*. [2012] and this study are significantly wider (Table 2) than those in the models presented by *Whittaker et al*. [2013] and *Williams et al*. [2011]. Table 2 also shows

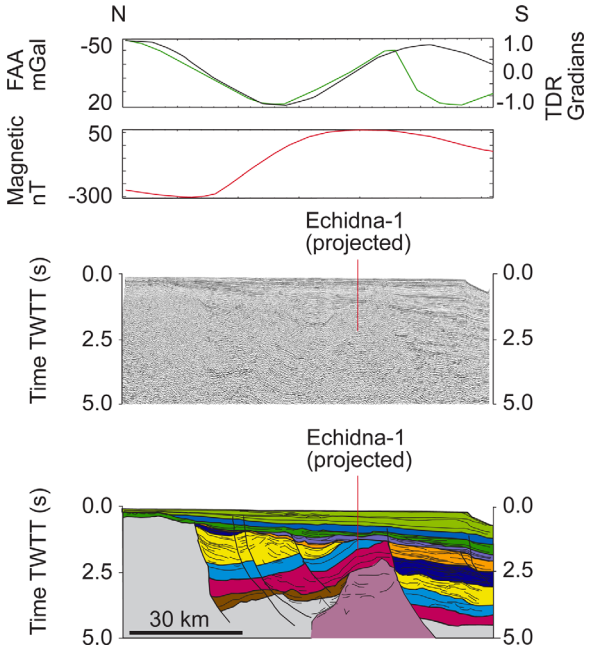

Figure 10. (a) Seismic line dh91–255 with the exploration well Echidna-1 projected ~4 km onto the line; The seismic example is accompanied by three profiles. Free-Air gravity anomalies (black); tilt derivative (green) and Reduced to the Pole magnetic anomalies (red).The stratigraphic interpretation is derived from *Totterdell et al*. [2000], modified by *Mantle et al*. [2009]. For the location of the seismic images see Figures 6 and 9a. Magnetic chron interpretations, (MQZB-c20o) come from *Tikku and Cande* [1999]. MQZB: Magnetic Quiet Zone Boundary. The seismic image used in this figure is published with permission from Fugro MCS.

how the widths of the margins and COTZs vary along strike. The timing of continental breakup is quite similar in those models that interpret a COTZ which could be interpreted as identifying the point of lithospheric breakup. Breakup is however older in models that are based on the first magnetic isochron identification or the assumption that mantle exhumation forms "new crust" created after crustal extension, which perhaps should be more akin to identifying the timing of crustal breakup [*Whittaker et al*., 2013; *Williams et al*., 2011]. True distinctions are currently poorly constrained but the application of these different interpretations could impact palaeoheat flow and subsidence modeling implications of the Australian and Antarctic margins.

[37] The COB presented in this study suggests that breakup processes were diachronous along the Australian and Antarctic margins, indicating some propagation or obliquity of opening (Table 3). In detail, our tabulated results suggest, but do not prove, that rifting propagated eastward within the transform margin with breakup not occurring until 65–52 Ma within the eastern sector of this study where the Bight and Otway basins meet (Figure 5).

[38] Finally we estimate, based on the inferred COTZs presented here and by *Direen et al*. [2012], what the likely extension rates were assuming steady extension between the inferred initiation of the COTZ and first breakup (Table 3). These estimates are tested within the plate kinematic models of *Whittaker et al*. [2013] and *Williams et al*. [2011]. The late-rift stage extension rates of the *Whittaker et al*. [2013] model are 18–25 mm/yr within the centre of the Australian-Antarctic plate boundary zone (Table 3). Rates of this order are observed in magmatic rifts near rupture [e.g., *Vigny et al*., 2006; *McClusky et al*., 2010], but are as yet undocumented for amagmatic or weakly magmatic margins. Using the kinematic model of *Williams et al*. [2011] COTZ extension rates are estimated at 5–11 mm/yr, within the range of rates associated with mantle exhumation, whereas the faster rates suggest a mean melt thickness on the order of 3–5 km across the Australian and Antarctic margins assuming a mantle potential temperature of 1300°C [*Pérez-Gussinyé et al*., 2006]. Within all the current extensional models the extension rate was greatest within the centre of the Australian-Antarctic margin, and significantly slower to the east. Further discussion of the extension rates, magmatic presence and the timing of extension is considered later.

5.2. Rift Localization by Melt Supply

[39] Many recent papers follow the seismic and 2-D gravity and magnetic model interpretations of *Sayers et al*. [2001] and argue for the presence of a basement ridge of unroofed serpentinized peridotites in the distal parts of the rift zone. Although not uniquely possible from the data over those parts of the rift zone, this interpretation is consistent with the dredging of mantle peridotites and basalts from the Diamantina Zone to the west (Figure 1) [*Nicholls et al*., 1981; *Chatin et al*., 1998; *Beslier*, 2004] and of where serpentinized peridotites, dolerites, gabbros and crustal rocks were returned from the Terre Adélie Ridge to the southeast (Figure 1) [*Tanahashi et al*., 1997; *Yuasa et al*., 1997]. Owing in part to the absence of basement samples from the central sector of the margin, multiple interpretations of 2-D seismic reflection and gravity profiles have suggested the presence of gabbroic intrusions, volcanic complexes, and blocks of continental crust alongside

that of serpentinized peridotite [*Eittreim and Smith*, 1987, *Eittreim*, 1994, *Sayers et al*., 2001; *De Santis et al*., 2003; *Colwell et al*., 2006; *Direen et al*., 2007, 2011, 2012].

[40] We use the seismic and magnetic calibrations of 3-D products of merged marine and onshore gravity data to provide an integrated model of margin formation. Our methods differ from those based solely on magnetic anomaly patterns, in that additional conditions are required to confirm the onset of seafloor spreading. We use the spatial distribution and shapes of basement highs, the presence or absence of high-density bodies on one or both margins, and their correlation with large offset or cannibalized sequences. As outlined below, our preferred interpretation of the integrated seismic reflection, gravity and magnetic data is that, 10–20 Myr prior to breakup, a significant number of magmatic bodies were emplaced or intruded within a narrow zone across both the Australian and Antarctic margins. As well as these magmatic intrusives, we allow for the possibility of zones of serpentinized peridotites within the COTZ in view of the variety of observable features in our integrated data set (Figures 8 and 9). In Figure 9a, we present our interpretations using a ~54 Ma reconstruction using the Euler rotation (25.06° about a pole at 36.0°E, 9.01°N) of *Whittaker et al*. [2007].

[41] The opaque basement bodies in seismic reflection data crossing the distal margin are not stratigraphically bound, having no obvious bases. Our new seismic mapping of the distribution of bodies shows that they mostly occur between the interpreted landward boundary of the COTZ and the COB (Figure 9a), with the exception of a few seismically defined bodies (e.g., Figure 10). Throughout the COTZ the crust is <10 km thick (Figure 5a) and dominantly populated by Phase 2 faults (Figures 5a, 6, and 11b), which are observed to be closely related to many of the individual opaque bodies (Figures 8a, 9b–9d, and 10). The seismic reflection observations of opaque bodies are mapped as a subset of higher confidence mafic body identifications. In addition we also interpret a less confident subset based on potential field data attributes alone.

[42] Mafic bodies were identified in the seismic data solely on the basis of reflection character and associations. On both margins, these bodies are identified from regions of opaque or chaotic seismic reflectivity that occur in close association with Phase 2 faults (e.g., Figures 8a, 8b, and 9c). Figures 8 and 9 show that these bodies generally correlate with positive anomalies in the tilt derivative and local increases over the background free-air anomaly. In detail, Figures 8 and 9 reveal more detail within this scheme. Some closely spaced seismically opaque bodies appear only as single peaks in the tilt derivative. Elsewhere, some larger and deeper bodies are only vaguely identifiable (e.g., Figure 8b) or only identifiable from tilt derivative peaks at their tips, perhaps because they present smaller density contrasts with their surroundings than shallower examples (e.g., Figure 8c). Despite the limitations of data resolution, we are able to extrapolate a number of these interpreted seismic-gravity bodies out into the gravity data set where no seismic data exist. Finally, a number of the seismic bodies also correlate with parts of the magnetic anomalies that have previously been interpreted as magnetic isochrons [e.g., *Tikku and Cande*, 1999].

[43] Based on these observations, we generated a regional interpretation of the distribution of mafic bodies in the Phase 2 rift zone by selecting parts of the potential field data sets that can be traced to a seismically defined opaque body and that meet at least one of the following criteria: (1) an identifiable (positive or negative) magnetic anomaly, (2) Euler solutions delineating a marked fault or step, and (3) a strong positive tilt derivative anomaly. Given its focus on potential field data, we expect this scheme of extrapolations to be biased to shallower mafic bodies.

[44] As introduced above, most of the interpreted opaque bodies lie within the MQZ (Figure 9a). This is particularly obvious within the eastern sectors and is dominant along the Antarctic margin, eastward of the isochron interpretations of *Tikku and Cande* [1999]; (Figure 9a). Others span the MQZ boundary, correlating with anomalies 34y, 33o, 27y, and 24o of *Tikku and Cande* [1999]. The presence of oblate bodies with similar seismic and gravity signatures each side of the MQZ boundary suggests that the interpretations of *Tikku and Cande* [1999] may be oversimplified. Similar correlations of features in extended continental crust with apparent magnetic isochrons were proposed by *Sibuet et al*. [2007] for the Newfoundland-Iberian rift and by *Sayers et al*. [2001] for the Australian margin.

[45] *Totterdell and Bradshaw* [2004] and *Schofield and Totterdell* [2008] argued that the presence of overmature organic material including coke from the Echidna-1 well (Figure 10) was sufficient evidence that the well was drilled close to a large

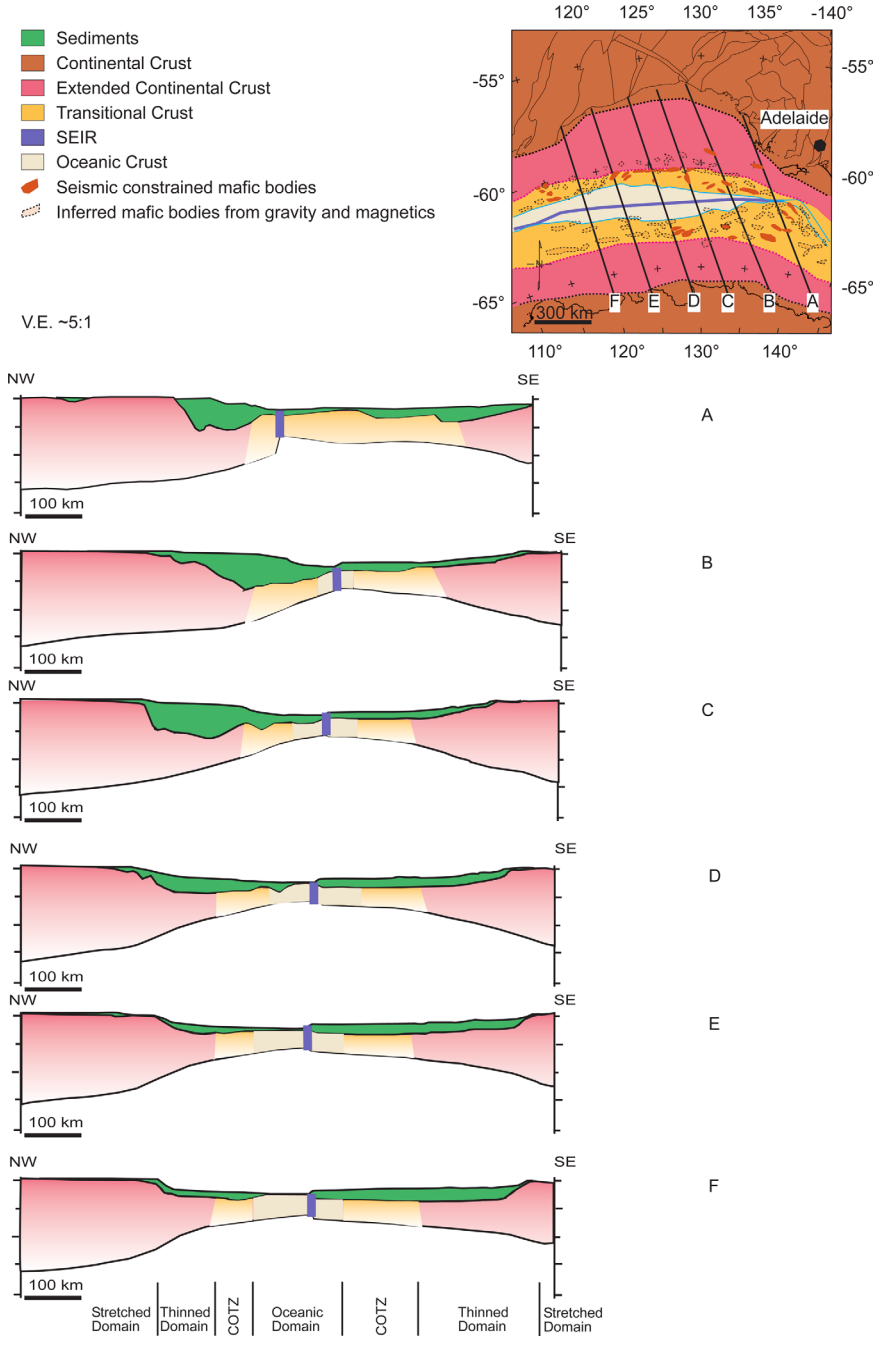

Figure 11. (a–f) Regional crustal profiles extracted from Australia and Antarctica after the grids have been clipped and rotated to c24o (53 Ma) using the Euler pole of rotation from *Whittaker et al*. [2007]. Antarctica is held in present-day position. The profiles extracted from the following grids: gridded bathymetry [*Sandwell and Smith*, 1997], sediment thickness (see text) and depth to Moho from gravity inversion (see text). Inset map shows the location of the profiles. Major crustal interpretations have been plotted on to the map delineating areas offshore interpreted as oceanic, transitional and continental crust. Onshore crustal elements after *Shaw et al*. [1996]. Inset map projection: Universal Polar Stereographic (median longitude 130°E).

magmatic intrusion. Large unconformities identified within the seismic data suggest uplift and erosion has occurred making it difficult to constrain the exact timing of the intrusion. The deformation of the Bronze Whaler (140–107 Ma) and Blue Whale (107–98.5 Ma) lead us to suggest that the intrusive body (Figure 10) was emplaced and/or intruded close to ~100–93.5 Ma. The younger age

constraint is derived from the presence of the Tiger sequence (93.5–84 Ma) tentatively interpreted above the observed unconformity (Figure 10). Regarding the possible arrival age of magmatic bodies this interpretation does not contradict our regional mapping of other seismically defined opaque basement bodies. Assuming the magnetic isochron interpretations [e.g., *Tikku and Cande*, 1999] can be used as pseudochrons the fact that some bodies lie landward of chron 34y and the magnetic quiet zone boundary (MQZB) suggests that they are older than 83.5 and 95 Ma respectively (Figures 9a–9c, and 9e). This assumed relationship does not however provide an absolute first arrival date for potential magma within the Australian-Antarctic rift. Within the constraints of the data available to us we suggest that possible magmatic bodies first arrived at ~100–93.5 Ma as rifting localized and strain reorganized between Australia and Antarctica.

[46] Structural and stratigraphic patterns suggest that magmatic intrusion may have occurred multiple times in some sectors and with distinct along-strike diachroneity after the initial pulse at 100–93.5 Ma. An eastward-younging pattern is proposed through the interpretation of sequential faulting and the formation of new border faults deforming older basin sequences (Figure 6). The variations in geophysical signatures imply differences in composition and/or emplacement (Figures 8–10). The acoustically opaque bodies have no consistent relationship with Phase 2 faults. Locally, Phase 2 faults in attenuated crustal blocks appear to sole out on the upper surfaces of opaque bodies below them (Figures 8b and 8c). These opaque bodies are therefore interpreted as gabbroic intrusives [e.g., *Thybo and Nielsen*, 2009], or alternatively as upper mantle rocks or serpentinite beneath embrittled lower crust [*White et al*.,1987; *Ebbing et al*., 2006; *Osmundsen and Ebbing*, 2008; *Mjelde et al*., 2009; *Lundin and Doré*, 2011]. Figure 9c shows an example of a mafic body that intruded or was exhumed along the footwall of a Phase 2 border fault. Figure 8c may show serpentinized mantle emplaced by low-angle shear at the base of a local detachment upon which large Phase 2 border faults detach. Other mafic bodies are located within the hanging walls of Phase 2 border faults, where they cross-cut pre-Tiger strata (i.e., older than 94 Ma) and so are interpreted as intrusives (Figures 8a, 9b, 9d, and 9e); others still are located at depth within the attenuated crust (Figures 8b and 8c). Elaborating this picture of variability, some of the bodies exhibit smooth upper surfaces (Figures 8b and 8c), leading to hypotheses that emplacement occurred locally along low-angle faults, whereas others have rugged tops more suggestive of volcanic construction (Figure 8a).

[47] Within the limitations of the data used to make them, therefore, our observations suggest that prolonged breakup processes along the Australian-Antarctic margins may have involved magma intrusion episodes without large volume eruptions leading to the formation of seaward-dipping volcanic sequences. Moreover, it is possible that melt products first appeared in the older, hitherto essentially amagmatic, rift system at approximately 100 Ma, at least 10–20 Myr before even the oldest estimates for the onset of seafloor spreading. The mapped mafic structures are individually up to 60 km long and changes in their orientations demarcate a 300–400 km scale segmentation of the COTZ (Figure 9a and Table 2). This pattern is similar to that observed along the eastern North American continental margin, where it is attributed to variability in melt supply to the COTZ by small-scale convection above the mantle transition zone [*Behn and Lin*, 2000].

5.3. Basement Influences on Rifting and Breakup

[48] Six regional crustal profiles (Figures 11a–11f) built from the reconstructed ~53 Ma gridded data sets (bathymetry, sediment thickness and crustal thickness) reveal the crustal architecture and along-strike variability of margin morphology. The most striking features are the asymmetrical COTZs and sediment thicknesses, and the apparently thinner crust of the Antarctic margin profile, which terminates at the ice shelf. The steeper predicted Moho beneath the Australian margin indicates how, according to our model, crustal thinning there was focussed into a narrower zone than for Antarctica. Considering that the Antarctic margin continues beneath the ice sheet, the comparison also demonstrates that our modeled Antarctic COTZ is broader than its Australian counterpart. It is also apparent that this asymmetry increases eastward within the Adélie Rift sector, as was also identified by *Colwell et al*. [2006] and *Close et al*. [2007].

[49] Within the distal margins we delineate five first-order segments originating within the transitional crust delineated by the Phase 2 faults and mafic bodies, summarized from west to east here in the rotated and restored reference frame of the Australian margin (Figures 3–6). Two segments

with W-E and NE-SW trends lie between 112° and 124°E. A third, central, segment at 124°–130°E, is wide and correlates with a broad W-E trending gravity anomaly on both margins. The fourth segment (130E–132.5E) hosts both W-E and NE-SW trending structures. The change from W-E to dominantly NW-SE structural trends of both Phase 1 and Phase 2 faults corresponds to the landward projection of the western boundary of this fourth segment, which roughly coincides with the border of the Gawler-Mawson Craton, Australia. The fifth (132.5E–137.5E), easternmost segment is dominated by NW-SE trends and its eastern border coincides with projections of the eastern margin of the Gawler-Mawson Craton and of the Spencer Fracture Zone (Figure 1). Within segments four and five, a NW-SE trending line of Euler solutions and tilt derivative anomaly (A4) occurs near the projected southern boundary of the Gawler-Mawson Craton (Figures 4b and 4c). It is possible therefore that this NW-SE trend is inherited from the Gawler-Mawson Craton, or it is derived from the early rifting process of the Gawler-Mawson Craton. Mechanical heterogeneity at the edge and within the Gawler-Mawson Craton may have dictated the location of a broad accommodation zone in the Phase 2 rift and ensuing SEIR.

[50] At the sector scale (≥300–400 km), along-axis segmentation of the COTZ may have been controlled by prerift lithospheric mechanical and compositional heterogeneities (Figure 9a and Table 2). Finally, we find no evidence for faults of large displacement or density contrasts highly oblique to the rift trend, arguing against the initiation of transform fault boundaries at segment terminations during Phase 1 or Phase 2 rifting. The absence of a transform signal suggests that changes in the relative motion of Australia and Antarctica occurred following the breakup of the Bight-Wilkes sector of the Australian-Antarctic margins. Based on our interpretations this would be possible at 50 Ma but not before. This observation is in agreement with the plate kinematic model of *Williams et al*. [2011].

6. Discussion

[51] Fault populations delineated across the Australian margin show that strain was first localized along large offset border fault systems on the shallow shelf, and along the shelf edge. The spatial offset in the crustal thinning oceanward of the Phase 1 border faults suggests progressive thinning along deeply buried faults and/or lower crustal flow occurred in response to stretching and surface loading. Seaward of the sharp change from >25 km thick crust to <15 km thick crust lies a younger, Phase 2 rift, suggesting a distinct localization of strain for a period prior to the onset of seafloor spreading, which occurred diachronously along the length of the Australian-Antarctic margins. Phase 1 basins are overprinted by structures of the younger rift (Phase 2). Multiple lines of evidence support temporally and spatially distinct phases of magmatism in this late-stage basin.

[52] Previous studies using 2-D seismic profiles have focussed on the inferred symmetry or asymmetry of the margins, and assumed that initial rift stage detachments remained the locus of strain throughout rifting [e.g., *Sayers et al*., 2001; *Direen et al*., 2011, 2012; *Espurt et al*., 2012]. Our interpretations, instead, indicate that a new system of faults formed late in the rift history; these faults may therefore penetrate an earlier detachment surface and even reuse local detachments at the base of the evolving crust. In other cases the presence of oblate mafic bodies along some of the later stage faults suggests that these faults probably penetrate the entire brittle crust.

[53] In the west, the margins are documented to be asymmetric between the Naturaliste Plateau and Bruce Rise sector [*Borrisova*, 2002]. In the east, the Otway-Adélie sector also appears to be highly asymmetric [*Stagg and Reading*, 2007; *Direen et al*., 2012]. The intervening Wilkes-Bight sector has been proposed to be symmetrical [e.g., *Sayers et al*., 2001; *Direen et al*., 2012]. Our analysis however reveals that the central sector is also asymmetric. Along the strike of the central Wilkes-Bight basin, the asymmetry is expressed in the variable widths of Phase 1 and Phase 2 rift zones. A fundamental limitation is the paucity of data beneath the Antarctic ice shelf and sheet; in particular, perched half-graben structures typical of many rifted margins are nowhere identified on the Antarctic margin [e.g., *Alves et al*., 2006; *Osmundsen et al*., 2002; *Unternehr et al*., 2010; *Zalán et al*., 2011]. Furthermore, the 3-D crustal architecture shows that the magnitude of thinning varies along strike and along each margin and that the crustal thinning gradients are steeper on the Australian margin. Some of the along-strike changes in the orientations of major faults and depocentres, as well as the locus of strain appear to be controlled by prerift lithospheric-scale heterogeneities, such as the NW-striking structures along the southern margin of Gawler-Mawson Craton. The along-strike change from a normal to

a transtensional margin was guided by the strong contrast in lithospheric properties across the boundary of the Gawler Craton and eastern Phanerozoic fold belts. The slow propagation of the ridge tip may indicate that the Gawler-Mawson Craton acted as a barrier to ridge propagation. The propagation barrier to the ridge tip may have locally enhanced the supply of decompressional melt [e.g., *Franke*, 2012] or alternatively have provided a mechanism for off-axis volcanism and magmatic activity during the early (~83–50 Ma) propagation of the ridge tip between Australia and Antarctica.

[54] What remains unclear in this new scheme is whether the older rift system was actively extending up until the time of rift localization. A relatively narrow zone of pronounced crustal thinning broadly separates the two rifts, and so may date to 145–100 Ma. Without tighter constraints on crust and upper mantle velocities and deeper imaging, one can only speculate on the mode(s) of extension within the mid to lower crust during rift evolution [e.g., *Lavier and Manatschal*, 2006; *Huismans and Beaumont*, 2008; *Thybo and Nielsen*, 2009].

[55] A close temporal relationship between strain localization and the initiation of magmatism in a narrow, central rift zone indicates the increasing role of mantle dynamics as rifting progresses to plate rupture [e.g., *Keir et al*., 2009; *Keranen et al*., 2009; *Yamasaki and Gernigon*, 2009]. Magmatism is not a prerequisite to the localization of rifting [e.g., *Cowie et al*., 2005], but we suggest that heat and volatile transfer from magmatic intrusions into the thinned crust approximately 60 Myr after rifting initiated could have accelerated plate weakening [e.g., *Buck*, 2004]. In the Bight basin, we also speculate that the Bight-Wilkes and northern Otway-Adélie margin sectors may have experienced enhanced melt production from a fertile mantle wedge following the subduction of the palaeo-Pacific lithosphere along the eastern seaboard of east Gondwana, which ended at ~100 Ma [*Gurnis and Müller*, 2003].

[56] Significant along-strike variations in the breadth and asymmetry of margins and the role of magmatism are observed in Earth's youngest rifted margins. The Salton Trough-Gulf of California [e.g., *Oskin et al*., 2001; *Lizarralde et al*., 2007] and the Gulf of Aden [*d'Acremont et al*., 2005; *Autin et al*., 2010] rift zones have profound along-strike variations between sectors separated by large offset fracture zones. In the gulfs of Aden and California the presence or absence of melt plays a vital role in how late syn-rift strain is accommodated providing a mechanism whereby mantle exhumation and magmatic segments occur in close proximity [*Lizarralde et al*., 2007; *Leroy et al*., 2010].

[57] Although we recognize the significance of magmatism during the late stages of continental rifting contributing to a complex COTZ, magmatic products are volumetrically minor, and so can only locally have accommodated significant extension. Based on the estimated extension rates for the COTZ (Table 3) within the kinematic model of *Williams et al*. [2011] we predict 3–5 km of additional melt under normal mantle conditions. The composition of the mafic bodies is not known from sampling, but both this new view and previous ones can be supported by geophysical interpretation and by analogy to comparable tectonic settings. Recent studies of the Norwegian margin have challenged the widely accepted interpretation of the high-velocity lower crust as a gabbroic underplate, suggesting instead that it may be serpentinized peridotite or intruded high-grade metamorphic rocks [*White et al*., 1987; *Ebbing et al*., 2006; *Osmundsen and Ebbing*, 2008; *Mjelde et al*., 2009; *Lundin and Doré*, 2011]. Along the Alpine-Tethys margins, magmatic arrival is estimated to precede seafloor spreading by 12–17 Myr but post-date the onset of rifting by 55–60 Myr [*Manatschal and Müntener*, 2008]. Similarly magma is documented to have arrived ~16 Myr before seafloor spreading but 55–72 Myr after rift onset along the Iberian-Newfoundland margins [*Whitmarsh et al*., 2000; *Boillot and Froitzheim*, 2001; *Péron-Pinvidic et al*., 2007]. Between Norway-Jan Mayen and Greenland multiple rift events occurred over 345–350 Myr yet magma is documented to have arrived only 5–6 Myr before seafloor spreading [*Roberts et al*.,1999; *Skogseid et al*., 2000; *Gaina et al*., 2009].

7. Conclusions

[58] Prerift reconstructions of the Australian and Antarctic plates and tectonic domains mapped from our potential field studies show that the initial rift developed preferentially within Proterozoic-Phanerozoic lithosphere, and its E-W trend was deflected around the present-day Gawler-Mawson Craton, leading to the development of an oblique rift zone. Between 165 and 145 Ma, regional extension led to the development of a

broad rift zone of numerous half graben, but with no evidence for syn-rift magmatism. By ~100 Ma, a new localized rift zone developed within the most extended part of the ever-broadening rift zone; new faults developed, producing a late-rift stage along-axis segmentation, and overprinting older structures. By 93.5 Ma, strain within this narrower zone was accommodated by both mechanical stretching and, we infer, localized magma intrusion in the attenuated crust. The new weakly magmatic rift developed rapidly in the E-W parts of the rift zone, but propagation of breakup was protracted in the transtensional Otway-Adélie sector where structures with NW-SE-striking structures during initial rifting. Propagation of the young mid-ocean ridge appears to have been extremely slow in this oblique rift sector.

[59] The spatial migration of rifting and the development of a new along-axis segmentation superposed on early rift-stage structures argue against prolonged extension having been localized along crustal and/or lithospheric detachments that developed during the early stages of rifting. Instead, observations of the conjugate Australian and Antarctic margins indicate that early syn-rift border faults were abandoned during late-stage rifting when a new segmentation pattern developed. Intrusive magmatism occurred in some of these late-stage rift segments, whereas in others large offset faults sequentially accommodated strain, locally, possibly, exposing upper mantle peridotites, until seafloor spreading processes initiated. The superposition of these processes and prolonged duration of rifting produced a broad zone of heterogeneous, transitional crust. Through seismic and gravity calibrations of the magnetic anomaly patterns, we interpret rift parallel magnetic anomalies as evidence for shallow mafic bodies (exhumed mantle, intrusive bodies) into stretched continental crust, with the first seafloor spreading anomaly as 34y (83.5 Ma) in the west, and 24o (53 Ma) in the east, or Otway basin region. We argue that the first-order (Proterozoic and Palaeozoic) lithospheric heterogeneities coupled with the time-space patterns of rift migration and W to E propagation, late-stage magmatism and sequential faulting combine to produce variable marginal asymmetries along this deepwater passive margin.

Acknowledgments

[60] Royal Holloway University of London for provision of the Thomas Holloway Scholarship and Geoscience Australia for funding and data. The original work that forms the basis of this paper was accepted by the University of London in 2005, supervised by C. Ebinger and K.McClay. Matthew J. Harvey is thanked for his critical proof reading of an earlier version of this manuscript. Comments gained by Tim Minshull, anonymous reviewers, and the editor greatly improved the original manuscript. J. Totterdell publishes with the permission of the Chief Executive Officer, Geoscience Australia. Australian seismic images are published with the permission of Fugro MCS. The Antarctic seismic images are published and available thanks to http://www.scar-sdls.org, the principal Antarctic library for seismic data, and the National Geophysical Data Center, NESDIS, NOAA, http://maps.ngdc.noaa.gov/viewers/geophysics/. Publication of the manuscript was supported by the Fault Dynamics Research Group, Royal Holloway University of London, UK, and ConocoPhillips.

References

Angelo, R. M. (2011), The identification of the ocean-continent transition at sediment-rich rifted continental margins: Northern Angola and Southern Australia rifted margins, PhD Thesis, pp. *189*, Univ. of Liverpool, U. K.

Alves, T. M., C. Moita, T. Cunha, J. H. Monteiro, and L. Pinheiro (2006), Meso-cenozoic evolution of North-Atlantic continental slope basins: The Peniche basin, Western Iberian margin, *AAPG Bull.*, *90*, 31–60.

Australian Survey (2001), GA228-24, http://www.scar-sdls.org.

Autin, J., S. Leroy, M.-O. Beslier, E. d'Acremont, P. Razin, A. Ribodetti, N. Bellahsen, C. Robin, and K. Al Toubi (2010), Continental breakup history of a deep magma-poor margin based on seismic reflection data (northeastern Gulf of Aden margin, offshore Oman), *Geophys. J. Int.*, *180*, 501–519, doi:10.1111/j.1365-246X.2009.04424.x.

Ball, P. J. (2005), Breakup history and evolution of the Southern passive margin of Australia, PhD Thesis, pp. *432*, R. Holloway, Univ. of London, U. K.

Bassi, G. (1995), Relative importance of strain rate and rheology for the mode of continental extension, *Geophys. J. Int.*, *122*, 195–210.

Behn, M. D., and J. Lin (2000), Segmentation in gravity and magnetic anomalies along the U.S. East coast passive margin: Implications for incipient structure of the oceanic lithosphere, *J. Geophys. Res.*, *105*(B11), 25,769–25,790.

Beslier, M.-O., et al. (2004), Une large transition continent-océan en pied de marge sud-ouest australienne: Premiers résultats de la campagne MARGAU/MD110, *Bull. Soc. Geol. Fr.*, *175*, 629–641.

Blevin, J. E. (2005), Geological framework of the Bremer and Denmark sub-basins, southwest Australia, R/V southern surveyor survey SS03/2004, Geoscience Australia Survey 265, post-survey report and GIS, Geoscience Australia Record 2005/05.

Blevin, J. E., and D. Cathro (2008), Project GA707, Client Report to Geoscience Australia by FrOG Tech Pty Ltd, 104 pp.

Boillot, G., and N. Froitzheim (2001), Nonvolcanic rifted margins, continental breakup and the onset of sea-floor spreading: Some outstanding questions, in *Nonvolcanic Rifting of Continental Margins: Evidence from Land and Sea*, edited by R. C. L. Wilson, R. B. Whitmarsh, B. Taylor, and N. Frotzheim, pp. 9–30, Geol. Soc. Spec. Publ. 187, London.

Bronner, A., D. Sauter, G. Manatschal, G. Péron-Pinvidic, and M. Munschy (2011), Magmatic breakup as an explanation for magnetic anomalies at magma-poor rifted margins, *Nat. Geosci.*, *4*, 549–553, doi:10.1038/NGEO12201.

Borissova, I. (2002), *Geological framework of the naturaliste plateau, Geosci. Aust. Rec., 2002/20*, Geosci. Aust., Australia.

Bradshaw, B. E, D. J. Ryan, C. J. Nicholson, R. P. D. O'Leary, C. J. Boreham, B. B. Hardy, R. W. Howe, F. Kroh, C. Mitchell, and E. Monteil (2005), Geology and petroleum potential of the bremer sub-basin, Offshore Southwestern Australia, Geoscience Australia Record 2005/21, Canberra, Australia.

Brown, B. J., R. D. Müller, and H. I. M. Struckmeyer (2001), Anomalous tectonic subsidence of the southern Australian passive margin: Response to Cretaceous dynamic topography or differential lithospheric stretching?, in *Eastern Australian Basin Symposium, A Refocused Energy Perspective for the Future*, in The Australasian Institute of Mining and Metallurgy, edited by K. C. Hill and T. Bernecker, Carlton, 25–28 November 2001, Melbourne, Victoria, pp. 563–569, Special publication/Petroleum Exploration Society of Australia.

Brown, B. J., R. D. Müller, C. Gaina, M. I. M. Struckmeyer, H. J. M. Stagg, and P. A. Symonds (2003), Formation and evolution of Australian passive margins: Implications for locating the boundary between continental and oceanic crust, in *Evolution and Dynamics of the Australian Plate*, vol. *372*, edited by R. R. Hillis, and R. D. Müller, pp. 223–244, Geol. Soc. Am., Spec. Pap, 372, pp. 223–243; doi: 10.1130/0-8137-2372-8.223.

Brun, J. P., and M.-O. Beslier (1996), Mantle exhumation at passive margins, *Earth Planet. Sci. Lett.*, *142*, 161–173.

Brune, S., A. A. Popov, and V. Sobolev (2012), Modeling suggests that oblique extension facilitates rifting and continental breakup, *J. Geophys. Res.*, *117*, B08402, doi:10.1029/2011JB008860.

Buck, W. R. (2004), *Consequences of athenospheric variability on continental rifting, in Rheology and Deformation of the Lithosphere at Continental Margins*, edited by G. D. Karner, B. Taylor, N. Driscoll, and D. Kohlstedt, pp. 1–30, Columbia Univ. Press, New York.

Cande, S. C., and J. C. Mutter, (1982), A Revised Interpretation of Seafloor Spreading Magnetic Anomalies between Australia and Antarctica, *Earth and Planet. Sci. Lett., 58*, p. 151–160.

Chatin, F., U. Robert, R. Montigny, and H. Whitechurch (1998), *La zone diamantine (ocean Indien oriental), temoin de la separation entre l'Australie and l'Antarctique: Arguments petrologique et geochimique*, C. R. Acad. Sci. Paris, *326*, 839–845.

Childs, J. R., and H. M. J. Stagg (1987), The deep crustal structure of the Wilkes land continental margin, in *Geology and Geophysics of Offshore Wilkes Land, Earth Science, series 5A*, edited by S. L. Eittreim, and M. A. Hampton, pp. 99–116, Circum-Pacific Counc. for Energy and Miner. Resour., Houston.

Christie, D. M., D. G. Pyle, R. B. Pedersen, and D. J. Miller (2004), Leg 187 synthesis: Evolution of the Australian Antarctic discordance, the Australian Antarctic depth anomaly, and the Indian/Pacific mantle isotropic boundary, in *Proceedings of the Ocean Drilling Program, Scientific Results*, vol. 187, edited by R. B. Pedersen, D. M. Christie, and D. J. Miller, pp. 1–41. [Available at http://www-odp.tamu.edu/publications/187_SR/187sr.htm, accessed 25 May 2013.].

Cleary, J. (1973), Australian crustal structure, *Tectonophysics*, *20*, 241–248.

Clitheroe, G., O. Gudmundsson, and B. L. N. Kennett (2000), The crustal thickness of Australia, *J. Geophys. Res.*, *105*(B6), 13,697–13,713.

Close, D. I., H. M. J. Stagg, and P. E. O'Brien (2007). Seismic stratigraphy and sediment distribution on the Wilkes Land and Terre Adélie margins, East Antarctica, *Mar. Geol.*, *239*, 33–57.

Close, D. I., A. B. Watts, and H. M. J. Stagg (2009), A marine geophysical study of the Wilkes land rifted continental margin, Antarctica, *Geophys. J. Int.*, *177*, 430–450, doi:10.1111/j.1365-246X.2008.04066.x.

Colwell, J. B., H. M. J. Stagg, N. G. Direen, G. Bernardel, and I. Borissova (2006), *The structure of the continental margin off Wilkes Land and Terre Adélie Coast, east Antarctica, in Antarctica: Contributions to Global Earth Sciences, chap. 6.6*, edited by D. K. Fütterer, D. Damaske, G. Kleinscmidt, H. Miller, and F. Tessensohn, pp. 327–340, Springer, New York.

Cooper, G. R. J., and D. R. Cowan (2006), Enhancing potential field data using filters based on the local phase, *Comput. Geosci.*, *32*, 1585–1591.

Corti, G., J. Van Wijk, M. Bonni, D. Skoutis, S. Cloetingh, F. Innocenti, and C. Manetti (2003), Transition from continental break-up to punctiform seafloor spreading: How fast, symmetric and magmatic, *Geophys. Res. Lett.*, *30*(12), 1604, doi:10.1029/2003GL017374.

Cowie, P. A., J. R. Underhill, M. D. Behn, J. Lin, and C. Gill (2005), Spatio-temporal evolution of strain accumulation derived from multi-scale observations of Late Jurassic rifting in the northern North Sea: A critical evaluation of models for lithospheric extension, *Earth Planet. Sci. Lett.*, *234*, 401–419.

Davis, M., and N. Kusznir (2004), Depth-dependent lithospheric stretching at rifted continental margins, in *Rheology and Deformation of the Lithosphere at Continental Margins,* edited by G. D. Karner, B. Taylor, N. Driscoll, and D. L. Kohlstedt, pp. 92–137, Columbia Univ. Press, New York, N. Y.

d'Acremont, E., S. Leroy, M. O. Beslier, N. Bellahsen, M. Fournier, C. Robin, M. Maia, and P. Gente (2005), Structure and evolution of the eastern Gulf of Aden conjugate margins from seismic reflection data, *Geophys. J. Int.*, *160*, 869–890.

Danesi, S., and A. Morelli (2000), Group velocity of Rayleigh waves in the Antarctic region, *Phys. Earth Planet. Inter.*, *122*, 55–66.

De Santis, L., G. Brancolini, and F. Donda (2003), Seismostratigraphic analysis of the Wilkes Land continental margin (East Antarctica): Influence of glacially driven processes on the Cenozoic deposition, *Deep Sea Res. Part II*, *50*, 1563–1594.

Direen, N. G., I. Borissova, H. M. J. Stagg, J. B. Colwell, and P. A. Symonds (2007), Nature of the continent-ocean transition zone along the southern Australian continental margin: A comparison of the Naturaliste Plateau, south-western Australia, and the central Great Australian Bight sectors, in *Imaging, Mapping and Modelling Continental Lithosphere Extension and Breakup*, vol. 282, edited by G. Karner, G. Manatschal, and L. Pinheiro, pp. 235–261, Spec. Publ. Geol. Soc., London.

Direen, N. G., H. M. J. Stagg, P. A. Symonds, and J. B. Colwell (2011), Dominant symmetry of a conjugate southern Australian and East Antarctic magma-poor rifted margin

segment, *Geochem. Geophys. Geosyst.*, *12(2)*, Q02006, doi: 10.1029/22010GC003306.

Direen, N. J., H. M. J. Stagg, P. A. Symonds, and I. O. Norton (2012), Variations in rift symmetry: Cautionary examples from the Southern Rift System (Australia-Antarctica), in *Conjugate Divergent Margins*, vol. 369, edited by W. Mohriak, M. Nemcok, A. Danforth, and S. Sinha, pp. 1–20, Geol. Soc. Spec. Publ., London, doi:10.1144/SP369.4.

Drummond, B. J., and C. D. N. Collins (1986), Seismic evidence for underplating of the lower continental crust of Australia, *Earth Planet. Sci. Lett.*, *79*, 361–372.

Dunbar, J. A., and D. S. Sawyer (1989), How pre-existing weaknesses control the style of continental break-up, *J. Geophys. Res.*, *94*(B6), 7278–7292.

Ebbing, J., E. R. Lundin, O. Olesen, and K. Hansen (2006), The mid-Norwegian margin: A discussion of crustal lineaments, mafi c intrusions, and remnants of the Caledonian root by 3-D density modelling and structural interpretation, *Geol. Soc. London J.*, *163*, 47–59, doi:10.1144/0016–764905-029.

Ebinger, C. J., J. van Wijk, and D. Keir (2013), The time scales of continental rifting: Implications for global processes, in GSA Centennial Volume, edited by M. Bickford, in press.

Eittreim, S. L. (1994), Transition from continental to oceanic crust on the Wilkes-Adélie margin of Antarctica, *J. Geophys. Res.*, *99*(B12), 24,189–24,205.

Eittreim, S. L., and G. L. Smith (1987), Seismic sequences and their distribution on the Wilkes Land margin in *The Antarctic Continental Margin: Geology and Geophysics of Offshore Wilkes Land, Earth Sci. Ser., vol. 5A*, edited by S. L. Eittreim and M. A. Hampton, pp. 15–43, Circum-Pacific Counc. for Energy and Miner. Resour., Houston, Tex.

Eittreim, S. L., M. A. Hampton, and J. R. Childs (1985), Seismic reflection signature of Cretaceous continental breakup on the Wilkes Land Margin, Antarctica, *Science*, *229*, 1082–1084.

Elburg, M. A., and A. Soesoo (1999), Jurassic alkali-rich volcanism in Victoria (Australia): Lithospheric versus asthenospheric source, *J. Afr. Earth Sci.*, *29*, 269–280.

Espurt, N., J.-P. Callot, F. Roure, J. M. Totterdell, H. I. M. Struckmeyer, and R. Vially (2012), Transition from symmetry to asymmetry during continental rifting: An example from the Bight Basin-Terre Adélie (Australian and Antarctic conjugate margins), *Terra Nova*, *24*(3), 167–180, doi:10.11 11/j.1365–3121.2011.01055.x.

Ferguson, J., R. Arculus, and J. Joyce (1979), Kimberlite and kimberlitic intrusions of southeastern Australia: A review, *BMR J. Aust. Geol. Geophys.*, *4*, 227–241.

Fishwick, S., B. L. N. Kennett, and A. M. Reading (2005), Contrasts in lithospheric structure within the Australian craton-insights from surface wave tomography, *Earth Planet. Sci. Lett.*, *231*,163–176, doi:10.1016/j.epsl.2005. 01.009.

Fitzsimons, I. C. W. (2003), Proterozoic basement provinces of southern and southwestern Australia, and their correlation with Antarctica, in *Proterozoic East Gondwana: Supercontinent Assembly and Break-Up*, vol. 206, edited by M. Yoshida, B. F. Windley, and S. Dasgupta, pp. 93–130, Geol. Soc. Spec. Publ., London, U. K.

Franke, D., (2012). Rifting, lithosphere breakup and volcanism: Comparison of magma-poor and volcanic rifted margins, *Mar. Pet. Geol.*, *43*, 63–87. doi:10.1016/j.marpet geo.2012.11.0 03.

Foden, J., S. H. Song, M. Elburg, P. B. Smith, B. Van der Steldt, and D. Van Penglis (2002), Geochemical evolution of lithospheric mantle beneath S.E. South Australia, *Chem. Geol.*, *182*, 663–695.

Gaina, C., L. Gernigon, and P. J. Ball (2009), Paleocene-recent plate boundaries in the NE Atlantic and the formation of the Jan Mayen microcontinent, *J. Geol. Soc. London*, *166*, 1–16, doi:10.1144/0016–76492008-112.

Gaul, O. F., S. Y. O'Reilly, and W. L. Griffin (2003), Lithosphere structure and evolution in southeastern Australia, in The Evolution and Dynamics of the Australian Plate, edited by R. R. Hillis and R. D. Müller, pp. 185–201, Geol. Soc. Am. Spec. Pap. 372.

Gurnis, M., and R. D. Müller (2003), The origin of the Australian Antarctic discordance from an ancient slab and mantle wedge, in *The Evolution and Dynamics of the Australian Plate*, edited by R. R. Hillis and R. D. Müller, Geol. Soc. Am. Spec. Pap. 372.

Gurnis, M., R. D. Müller, and L. Moresi (1998), Dynamics of Cretaceous vertical motion of Australia and the Australian-Antarctic discordance, *Science*, *279*, 1499–1504.

Hawkins, L. V., J. F. Hennion, J .E. Nafe, and H. A. Doyle (1965), Marine seismic refraction studies on the continental margin to the south of Australia, *Deep Sea Res.*, *12*, 479–495.

Hayward, N., and C. Ebinger (1996), Variations in along-axis segmentation of the Afar Rift system, *Tectonics*, *15*, 244–257.

Hegarty, K. A., J. K. Weissel, and J.C. Mutter (1988), Subsidence history of Australia's Southern Margin: Constrains on basin models, *Am. Assoc. Pet. Geol. Bull.*, *72*(6), 615–633.

Hergt, J. M., D. W. Peate, and C. J. Hawkesworth (1991), The Petrogenesis of mesozoic gondwana low-Ti flood basalts, *Earth Planet. Sci. Lett.*, *105*, 134–148.

Huismans, R. S., and C. Beaumont (2008), Complex rifted continental margins explained by dynamical models of depth-dependent lithospheric extension, *Geology*, *36*, 163–166, doi:10.1130/G24231A.1.

Huismans, R. S., and C. Beaumont (2011), Depth-dependent extension, two-stage breakup and cratonic underplating at rifted margins, *Nature*, *473*, 74–78, doi:10.1038/nature 09988.

Keir, D., I. D. Bastow, K. A. Whaler, E. Daly, D. G. Cornwell, and S. Hautot (2009), Lower crustal earthquakes near the Ethiopian rift induced by magmatic processes, *Geochem. Geophys. Geosyst.*, *10*, Q0AB02, doi:10.1029/2009GC0 02382.

Keranen, K. M., S. L. Klemperer, J. Julia, J. F. Lawrence, and A. A. Nyblade, (2009), Low lower crustal velocity across Ethiopia: Is the main Ethiopian rift a narrow rift in a hot craton?, *Geochem. Geophys. Geosyst.*, *10*, Q 0AB01, doi:10. 1029/2008GC002293.

Konig, M. (1987), Geophysical data from the continental margin off Wilkes land, Antarctica-implications for breakup and dispersal of Australia and Antarctica, in *The Antarctic Continental Margin: Geology and Geophysics Offshore Wilkes Land, CPCEMR Earth Sci. Ser.,* 5A, edited by S. L. Eittreim and M. A. Hampton, pp. 117–116, Circum-Pacific Counc. for Energy and Miner. Resour., Houston, Tex.

Konig, M., and M. Talwani (1977), A geophysical study of the southern continental margin of Australia: Great Australian bight and western sections, *Geol. Soc. Am. Bull.*, *88*, 1000–10,014.

Krassay, A. A., D. L. Cathro, and D. J. Ryan (2004), A regional tectonostratigraphic framework for the Otway Basin, in *Eastern Australasian Basins Symposium II*, edited by P. J. Boult, D. R. Johns, and S. C. Lang, Petroleum Exploration

Society of Australia, Special Publication, pp. 97–116, Adelaide, South Australia, 19–22 September 2004, Petroleum Exploration Society of Australia.

Kusznir, N. (2009), *South Australia–Antarctica conjugate rifted margins: Mapping crustal thickness and lithosphere thinning using satellite inversion, Report for Geoscience Australia (unpublished),* https://www.ga.gov.au/products/servlet/controller?event=GEOCAT_DETAILS&catno=68655.

Laske, G., and G. Masters (1997), *A Global Digital Map of Sediment Thickness, EOS Trans*. AGU, *78*, F483.

Lavier, L., and G. Manatschal (2006), Mechanism to thin the continental lithosphere at magma poor margins, *Nature*, *440*, 324–328.

Leroy, S., et al. (2010), Contrasted styles of rifting in the eastern Gulf of Aden: A combined wide-angle, multichannel seismic, and heat flow survey, *Geochem. Geophys. Geosyst.*, *11*, Q07004, doi:10.1029/2009GC002963.

Lister, G. S., M. A. Etheridge, and P. A. Symonds (1986), Detachments faulting and the evolution of passive margins, *Geology*, *14*, 246–250.

Lizarralde, D., et al. (2007), Variation in styles of rifting in the Gulf of California, *Nature*, *448*, 466–469, doi:10.1038/nature06035.

Lundin, E. R., and A. G. Doré (2011), margin compressional deformation hyperextension, serpentinization, and weakening: A new paradigm for rifted margin compressional deformation, *Geology*, *39*, 347–350, doi:10.1130/G31499.1.

Manatschal, G. (2004), New models for evolution of magma-poor rifted margins based on a review of data and concepts from west Iberia and the Alps, *Int. J. Earth Sci.*, *93*, 432–466.

Manatschal, G., and O. Müntener (2008), A type sequence across an ancient magma-poor ocean–continent transition: The example of the western Alpine Tethys ophiolites, *Tectonophysics*, *473*, 4–19.

Mantle, D. J., J. M. Totterdell, H. I. M. Struckmeyer, and A. P. Kelman (2009), Bight basin biozonation and stratigrpahy, chart 35, Geosci. Aust., Australia. [Available at http://www.ga.gov.au/image_cache/GA14545.pdf, accessed 27 May 2013.].

Marson, I., and E. E. Klingele (1993), Advantages of using the vertical gradient of gravity for 3-D interpretation, *Geophysics*, *58*, 1588–1595.

Maus, S., et al. (2009), EMAG2: A 2-arc min resolution earth magnetic anomaly grid compiled from satellite, airborne, and marine magnetic measurements, *Geochem. Geophys. Geosyst.*, *10*, Q08005, doi:10.1029/2009GC002471.

McAdoo, D., and S. Laxon (1997), Antarctic tectonics: Constraints from an ERS-1 satellite marine gravity field, *Science*, *276*, 556–561.

McClusky, S., et al. (2010), Kinematics of the southern Red Sea-Afar triple junction and implications for plate dynamics, *Geophys. Res. Lett.*, *37*, L05301, doi:10.1029/2009GL041127.

McKenzie, D. (1978), Some remarks on the development of sedimentary basins, *Earth Planet. Sci. Lett.*, *40*, 25–32.

Mjelde, R., J. I. Faleide, A. Breivik, and T. Raum (2009), Lower crustal composition and crustal lineaments on the Vøring margin, NE Atlantic: A review, *Tectonophysics*, *472*, 183–193, doi:10.1016/j.tecto.2008.04.018.

Moore, G. W., and S. L. Eittreim (1987), Mechanism of extension and rifting at the Antarctica continental margin, in *The Antarctic Continental Margin: Geology and Geophysics of Offshore Wilkes Land, Earth Sci. Ser*., vol. 5a, edited by S. L. Eittreim and M. A. Hampton, pp. 89–97, Circum-Pacific Counc. for Energy and Miner. Resour., Houston, Tex.

Muntener, O., and G. Manatschal (2006), High degrees of melt extraction recorded by spinel harzburgite of the Newfoundland margin: The role of inheritance and consequences for the evolution of the southern North Atlantic, *Earth Planet. Sci. Lett.*, *252*, 437–452.

Nicholls, I. A., J. Ferguson, H. Jones, G. P. Marks, and J. C. Mutter (1981), Ultramafic blocks from the ocean floor southwest of Australia, *Earth Planet. Sci. Lett.*, *56*, 362–374.

O'Reilly, S. Y., and W. L. Griffin (2006), Imaging global chemical and thermal heterogeneity in the subcontinental lithospheric mantle with garnets and xenoliths: Geophysical implications, *Tectonophysics*, *416*, 289–309, doi:10.1016/j.tecto.2005.11.014.

Oldenburg, D. W. (1974), The inversion and interpretation of gravity anomalies, *Geophysics*, *39*, 526–536.

Oskin, M., J. M. Stock, and A. Martín-Barajas (2001), Rapid localization of Pacific-North America plate motion in the Gulf of California, *Geology*, *29*, 459–462.

Osmundsen, P. T., and J. Ebbing (2008), Styles of extension offshore mid-Norway and implications for mechanisms of crustal thinning at passive margins, *Tectonics*, *27*, TC6016, doi:10.1029/2007tc002242.

Osmundsen, P. T., A. Sommaruga, J. R. Skilbrei, and O. Olesen (2002), Deep structure of the Norwegian Sea area, North Atlantic margin, *Norw. J. Geol.*, *82*, 205–224.

Parker, R. (1972), The rapid calculation of potential field anomalies, *Geophys. J. R. Astron. Soc.*, *31*, 447–455.

Pérez-Gussinyé, M., T. Reston, and J. P. Morgan (2001), Serpentinization and magmatism during extension at nonvolcanic margins—The effect of initial lithospheric structure, in *Nonvolcanic Rifting of Continental Margins: Evidence From Land and Sea*, edited by R. C. L. Wilson, R. B. Whitmarsh, B. Taylor, and N. Froitzheim, pp. 551–576, Geol. Soc. Spec. Publ. 187, London.

Pérez-Gussinyé, M., J. P. Morgan, T. J. Reston, and C. R. Ranero (2006), From rifting to spreading at nonvolcanic margins: Insights from numerical modelling. *Earth Planet. Sci. Lett.*, *244*, 458–473.

Péron-Pinvidic, G., and G. Manatschal (2009), The final rifting evolution at deep magma-poor passive margins from Iberia-Newfoundlland: A new point of view, *Int. J. Earth Sci.*, *98*, 1581–1597, doi:10.1007/s00531-008-0337-9.

Péron-Pinvidic, G., G. Manatschal, T. A. Minshull, and D. S. Sawyer (2007), Tectonosedimentary evolution of the deep Iberia-Newfoundland margins: Evidence for a complex breakup history, *Tectonics*, *26*, TC2011, doi:10.1029/2006TC001970.

Petit, C., and C. Ebinger (2000), Flexure and mechanical behaviour of cratonic lithosphere: Gravity models of the East African and Baikal rifts, *J. Geophys. Res.*, *105*(B8), 19,151–19,162.

Petkovic, P. (2004), Time-depth functions for basins of the Great Australian Bight, *Geosci. Aust. Rec. 01/2004*, Geosci. Aust., Australia.

Petkovic, P., and P. Milligan (2002), *Magnetic Anomaly Grid of the Australian Region 3.1 [CD-ROM]*, Geosci. Aust., Canberra.

Petkovic, P., J. Brett, M. P. Morse, L. Hatch, M. A. Webster, and P. Roche (1999a), Gravity, magnetic and bathymetry grids from levelled data for southwest Australia-Southwest region, *AGSO Rec. 1999/47*, AGSO, Australia.

Petkovic, P., M. P. Morse, J. Brett, A. S. Murray, M. A. Webster, T. M. Grabovszky, T. E. Mackey, and P. Roche

(1999b), Gravity, magnetic and bathymetry grids from levelled data for northwest Australia, AGSO *Rec. 41/1999*, AGSO, Australia.

Petkovic, P., J. Brett, M. P. Morse, L. Hatch, M. A. Webster, and P. Roche (2001), Gravity, magnetic and bathymetry grids from levelled data for Southwest Australia-Great Australian Bight*, AGSO Rec., 48/2001*, AGSO, Australia.

Ranero, C. R., and M. Pérez-Gussinyé (2010), Sequential faulting explains the asymmetry and extension discrepancy of conjugate margins, *Nature*, *468*, 294–249, doi:10.1038/nature09520.

Reid, A. B., J. M. Allsop, H. Granser, A. J. Millett, and I. W. Somerton (1990), Magnetic interpretation in three dimensions using Euler deconvolution, *Geophysics*, *55*, 80–91.

Reston, T. (2007), Depth-dependent stretching or unrecognized faulting?, Extension discrepancy at North Atlantic nonvolcanic rifted margins, *Geology*, *35*, 367–370.

Reston, T., C. M. Krawczyk, and D. Klaescen (1996), The S reflector west of Galicia (Spain): Evidence for detachment faulting during continental break-up from prestack depth Migration, *J. Geophys. Res.*, *101*(B4), 8075–8091.

Ritzwoller, M. H., N. M. Shapiro, A. L. Levshin, and G. M. Leahy (2001), Crustal and upper mantle structure beneath Antarctica and surrounding oceans, *J. Geophys. Res.*, *106*(B12), 30,645–30,670.

Roberts, D. G., M. Thompson, B. Mitchener, J. Hossack, S. Carmichael, and H.-M. Bjørnseth (1999), Palaeozoic to Tertiary Rift and Basin Dynamics: Mid-Norway to the Bay of Biscay—A New Context for Hydrocarbon Prospectivity in *the Deep Water Frontier, Pet. Geol. Conference Ser.*, vol. *5*, pp. 7–40, Geol. Soc., London, doi:10.1144/0050007.

Salem, A., S. Williams, D. Fairhead, R. Smith, and D. Ravat (2008), Interpretation of magnetic data using tilt-angle derivatives, *Geophysics*, *73*, 1–10, doi:10.1190/1.2799992.

Sandwell, D. T., and W. H. F. Smith (1997), Marine gravity anomaly from Geostat and ERS-1 satellite altimetry, *J. Geophys. Res.*, *102*(B5), 10,039–10,054.

Sandwell, D. T., and W. H. F. Smith (2009), Global marine gravity from retracked Geosat and ERS-1 altimetry: Ridge segmentation versus spreading rate, *J. Geophys. Res.*, *114*, B01411, doi:10.1029/2008JB006008.

Sayers, J., P. Symonds, N. G. Direen, and G. Bernardel (2001), Nature of the continent-ocean transition on the non-volcanic rifted margin of the central Great Australian Bight, in *Non-Volcanic Rifting of Continental Margins: A Comparison of Evidence From Land and Sea*, vol. 187, edited by R. C. L. Wilson, R. B. Whitmarsh, and N. Froitzheim, pp. 51–76, Geol. Soc. Spec. Publ., London.

Scholfield, A., and J. Totterdell (2008), Distribution, timing and origin of magmatism in the Bight and Eucla basins, with implications for hydrocarbon prospectivity, Geoscience Australia Record, 2008/024, p. 19, Geosci. Aust., Australia.

Shaw, R. D., P. Wellman, P. Gunn, A. J. Whitaker, C. Tarlowski, and M. Morse (1996), *Guide to using the crustal elements map, AGSO Rec. 1996/30*, AGSO, Australia.

Sibuet, J.-C., S. Srivastava, and G. Manatschal (2007), Exhumation mantle-forming transitional crust in the Newfoundland-Iberia rift and associated magnetic anomalies, *J. Geophys. Res.*, *112*, B06105, doi:10.1029/2005JB003856.

Shillington, D. J., C. L. Scott, T. A. Minshull, R. A. Edwards, P. J. Brown, and N. White (2009), Black Sea Abrupt transition from magma-starved to magma-rich rifting in the eastern, *Geology*, *37*, 7–10. doi:10.1130/G25302A.1.

Simons, F. J., and R. D. van der Hilst (2002), Age-dependent seismic thickness and mechanical strength of the Australian lithosphere, *Geophys. Res. Lett.*, *29*(11), doi:10.1029/2002GL014962.

Simons, F. J., A. Zielhuis, and R. D. van der Hilst (1999), The deep structure of the Australian continent from surface wave tomography, *Lithos*, *48*, 17–43.

Skogseid, J., S. Planke, J. I. Faleide, T. Pedersen, O. Eldholm, and F. Neverdal (2000), NE Atlantic continental rifting and volcanic margin formation, pp. 295–326, Geol. Soc. Spec. Publ. 167, London.

Stagg, H. M. J., and A. M. Reading (2007), Crustal architecture of the oblique-slip conjugate margins of George V Land and southeast Australia, *in Antarctica: A Keystone in a Changing World – Online Proceedings of the 10th ISAES*, edited by A.K. Cooper and C.R. Raymond et al., USGS Open-File Report 2007-1047, *109*, 6 pp., doi:10.31 33/of2007-1047.srp109.

Stagg, H. M. J., J. B. Colwell, N. G. Direen, P. E. O'Brien, B. J. Brown, G. Bernardel, I. Borissova, L. Carson, and D. Close (2005), Geological framework of the continental margin in the region of the Australian Antarctic Territory, *Geosci. Aust. Rec. 2004/25*, Geosci. Aust., Australia.

Stavrev, P.Y. (1997), Euler deconvolution using differential similarity transformations of gravity or magnetic anomalies, *Geophys. Prospect.*, *45*, 207–246, doi:10.1046/j.1365–2478.1997.00331.

Stracke, K. J., J. Ferguson, and L. P. Black (1979), Structural setting of kimberlites in southeastern Australia, in *Kimberlites, Diatremes and Diamonds: Their Geology, Petrology and Geochemistry*, edited by F. R. Boyd, and H. O. A. Meyer, pp. 71–91, American Geophysical Union, Washington, D. C.

Talwani, M., J. Mutter, R. Houtz, and M. Konig (1978), The crustal structure and evolution of the area underlying the magnetic quiet zone on the margin of Australia, in *Geological and Geophysical Investigations of Continental Margins*, vol. *29*, edited by J. Watkins, L. Montadert, and P. Dickenson, pp. 151–175, Am. Assoc. of Pet. Geol. Mem, Tulsa, Okla.

Tanahashi, M., T. Ishihara, M. Yuasa, F. Murkami, and A. Nishimura (1997), Preliminary report of the TH95 geological and geophysical survey results in the Ross Sea and Dumont D'Urvills Sea, *Proc. NIPR Symp. Antarctica Geosci., 10*, 36–58.

Thybo, H., and C. A. Nielsen (2009), Magma-compensated crustal thinning in continental rift zones, *Nature*, *457* (7231), 873–876, doi:10.1038/nature07688.

Tiberi, C., M. Diament, H. Lyon-Caen, and T. King (2001), Moho topography beneath Corinth (Greece) rift from inversion of gravity data, *Geophys. J. Int.*, *145*, 797–808.

Tiberi, C., E. Ebinger, V. Ballu, G. Stuart, and B. Oluma (2005), Inverse models of gravity data from the Red Sea-Aden-East African rifts triple junction zone, *Geophys. J. Int.*, *163*, 775–787, doi:10.1111/j.1365-246X.2005.02736.x.

Tikku, A. A., and S. C. Cande (1999), The oldest magnetic anomalies in the Australian-Antarctic Basin: Are they isochrons?, *J. Geophys. Res.*, *104*(B1), 661–677.

Tikku, A. A., and N. G. Direen (2008), Comment on ''Major Australian-Antarctic Plate Reorganization at Hawaiian-Emperor Bend Time'', *Science*, *321*, 490.

Torsvik, T. H., L. M. Carter, L. D. Ashwal, S. K. Bhushan, M. K. Pandit, and B. Jamtveit (2001), Rodinia refined or obscured: Palaeomagnetism of the Malani igneous suite (NW India), *Precambrian Res.*, *108*, 319–333.

Totterdell, J. M., and B. E. Bradshaw (2004), The structural framework and tectonic evolution of the Bight Basin, in *Eastern Australasian Basins Symposium II*, edited by P. J. Boult, D. R. Johns, and S. C. Lang, pp. 41–61, 19–22 September 2004, Spec. Publ., Petroleum Exploration Society of Australia, Adelaide, South Australia.

Totterdell, J. M., J. E. Blevin, H. I. M. Struckmeyer, B. E. Bradshaw, J. B. Colwell, and J. M. Kennard (2000), A new sequence framework for the Great Australian Bight: Starting with a clean slate, *AAPEA J.*, *40*, 95–117.

Totterdell, J. M., B. E. Bradshaw, and J. B. Willcox (2003), Structural and tectonic setting of the Great Australian Bight, in *Petroleum Geology of South Australia*, vol. *5*, *Great Australian Bight*, edited by G. W. O'Brien, E. Paraschivoiu, and J. E. Hibburt, pp. 1–57, Primary Ind. and Resour., South Australia.

Unternehr, P., G. Péron-Pinvidic, G. Manatschal, and E. Sutra (2010), Hyper-extended crust in the South Atlantic: In search of a model, *Pet. Geosci.*, *16*, 207–215.

U.S. Geological Survey, Geophysical Survey L-1-84-AN (L184AN), National Geophysical Data Center, NESDIS, NOAA, http://maps.ngdc.noaa.gov/viewers/geophysics.

van Avendonk, H. J. A., L. L. Lavier, D. J. Shillington, and G. Manatschal (2009), Extension of continental crust at the margin of the eastern Grand Banks, Newfoundland, *Tectonophysics*, *468*, 131–148.

van Wijk, J. W., and D. K. Blackman (2005), Dynamics of continental rift propagation: End-member modes, *Earth Planet. Sci. Lett.*, *229*, 247–258.

Vauchez, A., G. Barruol, and A. Tommasi (1997), Why do continents break-up parallel to ancient orogenic belts?, *Terra Nova*, *9*, 62–66.

Vigny, C., P. Huchon, J.-C. Ruegg, K. Khanbari, and L. M. Asfaw (2006), Confirmation of Arabia plate slow motion by new GPS data in Yemen, *J. Geophys. Res.*, *111*, B02402, doi:10.1029/2004JB003229.

von Frese, R. R. B., L. Tan, L. W. Kim, and C. R. Bentley (1999), Antarctic crustal modelling from the spectral correlation of free-air gravity anomalies with the terrain, *J. Geophys. Res.*, *104*(B11), 25,275–25,296.

Wannesson, J. (1991), Geology and petroleum potential of the Adélie Coast margin, East Antarctica, in *Antarctica as an Exploration Frontier–Hydrocarbon Potential, Geology, and Hazards*, vol. *31*, edited by St. W. John, pp. 77–87, AAPG Stud. in Geol, Tulsa, Okla.

Wannesson, J., B. Pelras, M. Petiperrin, M. Perret, and J. Segoufin (1985), A geophysical transect of the Adélie margin, East Antarctica, *Mar. Pet. Geol.*, *2*, 192–201.

Weissel, J. K., and D. E. Hayes (1972), Magnetic anomalies in the Southeast Indian Ocean, in *Antarctic Research II: The Australian-New Zealand Sector, vol. 19*, edited by D. E. Hayes, pp. 165–196, AGU, Antarctic Res. Ser., Washington, D. C.

White, R. S., G. D. Spence, S. R. Fowler, D. P. McKenzie, G. K. Westbrook, and A. N. Bowen (1987), Magmatism at rifted continental margins, *Nature*, *330*, 439–444.

Whitmarsh, R. B., S. M. Dean, T. A. Minshull, and M. Tompkins (2000), Tectonic implications of exposure of lower continental crust beneath the Iberia Abyssal Plain, northeast Atlantic Ocean: Geophysical evidence, *Tectonics*, *19*, 919–942.

Whitmarsh, R. B., G. Manatschal, and T. A. Minshull (2001), Evolution of magma-poor continental margins from rifting to seafloor spreading, *Nature*, *413*, 150–153.

Whittaker, J. M., R. D. Müller, G. Leitcheenkov, H. Stagg, M. Sdrolias, C. Gaina, and A. Goncharov (2007), Major Australian-Antarctic plate reorganization at Hawaiian-Emperor bend time, *Science*, *318*, 83–86, doi:10.1126/science.1143769.

Whittaker, J. M., R. D. Müller, and M. Gurnis (2010), Development of the Australian-Antarctic depth anomaly, *Geochem. Geophys. Geosyst.*, *11*, Q11006, doi:10.1029/2010GC003276.

Whittaker, J. M., S. E. Williams, and R. D. Müller (2013), Revised tectonic evolution of the eastern Indian Ocean, *Geochem. Geophys. Geosyst.*, doi:10.1002/ggge.20120, in press. [Available at ftp://ftp.earthbyte.org/earthbyte/Whittaker-KerguelenPlateau/, accessed 27 May 2013.]

Williams, S. E., J. M. Whittaker, and R. D. Müller (2011), Full-fit, palinspastic reconstruction of the conjugate Australian–Antarctic margins, *Tectonics*, *30*, TC6012, doi:10.1029/2011TC002912. [Available at ftp://ftp.earthbyte.org/earthbyte/AustraliaAntarcticaReconstruction/, accessed 27 May 2013.]

Wyatt, B. A., S. R. Shee, W. L. Griffin, P. Zweistra, and H. R. Robinson (1994), The petrology of the Cleve kimberlite, Eyre Peninsula, South Australia, in *Diamonds: Characterization, Genesis, and Exploration*, edited by H. O. A. Meyer and O. H. Leonardos, pp. 51–68, CPRM Spec. Publ. IB/93, Brazilia, Brazil.

Yamasaki, T., and L. Gernigon (2009), Styles of lithospheric extension controlled by underplated mafic bodies, *Tectonophysics*, *468*, 169–184. [Available at http://dx.doi.org/10.1016/j.tecto.2008.04.024, Accessed 27 May 2013.].

Yuasa, M., K. Niida, T. Ishihara, K. Kisimoto, and F. Murakami (1997), Peridotite dredged from a seamount off Wilkes Land, the Antarctic: Emplacement of fertile mantle fragment at early rifting stage between Australia and Antarctica during the final breakup of Gondwanaland, in *The Antarctic Region: Geological Evolution and Processes*, edited by C. A. Ricci, pp. 7225–730, Terra Antarctica, Siena, Italy.

Zalán, P. V., M. do Carmo Garcia Severino, C. A. Rigoti, L. P. Magnavita, J. A. B. de Oliveira, and A. R. Vianna (2011), An Entirely New 3-D-View of the Crustal and Mantle Structure of a South Atlantic Passive Margin—Santos, Campos and Espírito Santo Basins, Brazil, 10 pp., AAPG Annual Convention, Houston, Tex., Extended Abstracts, Search and Discovery Article #30177.

Zuber, M. T., T. D. Betchel, and D. W. Forsyth (1989), Effective elastic thickness of the lithosphere and mechanisms of isostatic compensation, Australia, *J. Geophys. Res.*, *94*(B7), 9353–9367.